

# Journal Pre-proof

NO-releasing STAT3 inhibitors suppress BRAF-mutant melanoma growth

Tamer S. Kaoud, Aliaa M. Mohassab, Heba A. Hassan, Chunli Yan, Sabrina X. Van Ravenstein, Dalia Abdelhamid, Kevin N. Dalby, Mohamed Abdel-Aziz



PII: S0223-5234(19)31037-2

DOI: <https://doi.org/10.1016/j.ejmech.2019.111885>

Reference: EJMECH 111885

To appear in: *European Journal of Medicinal Chemistry*

Received Date: 14 September 2019

Revised Date: 12 November 2019

Accepted Date: 12 November 2019

Please cite this article as: T.S. Kaoud, A.M. Mohassab, H.A. Hassan, C. Yan, S.X. Van Ravenstein, D. Abdelhamid, K.N. Dalby, M. Abdel-Aziz, NO-releasing STAT3 inhibitors suppress BRAF-mutant melanoma growth, *European Journal of Medicinal Chemistry* (2019), doi: <https://doi.org/10.1016/j.ejmech.2019.111885>.

This is a PDF file of an article that has undergone enhancements after acceptance, such as the addition of a cover page and metadata, and formatting for readability, but it is not yet the definitive version of record. This version will undergo additional copyediting, typesetting and review before it is published in its final form, but we are providing this version to give early visibility of the article. Please note that, during the production process, errors may be discovered which could affect the content, and all legal disclaimers that apply to the journal pertain.

© 2019 Published by Elsevier Masson SAS.

## **NO-releasing STAT3 inhibitors suppress BRAF-mutant melanoma growth**

Tamer S. Kaoud<sup>a#</sup>, Aliaa M. Mohassab<sup>b#</sup>, Heba A. Hassan<sup>b</sup>, Chunli Yan<sup>c</sup>, Sabrina X. Van Ravenstein<sup>a</sup>,  
Dalia Abdelhamid<sup>b\*</sup>, Kevin N. Dalby<sup>a\*</sup> and Mohamed Abdel-Aziz<sup>b</sup>

<sup>a</sup> Division of Chemical Biology and Medicinal Chemistry, College of Pharmacy, the University of Texas at Austin, Austin, TX 78712, USA.

<sup>b</sup> Department of Medicinal Chemistry, Faculty of Pharmacy, Minia University, Minia 61519, Egypt.

<sup>c</sup> Department of Chemistry, Georgia State University, Atlanta, GA 30302, USA.

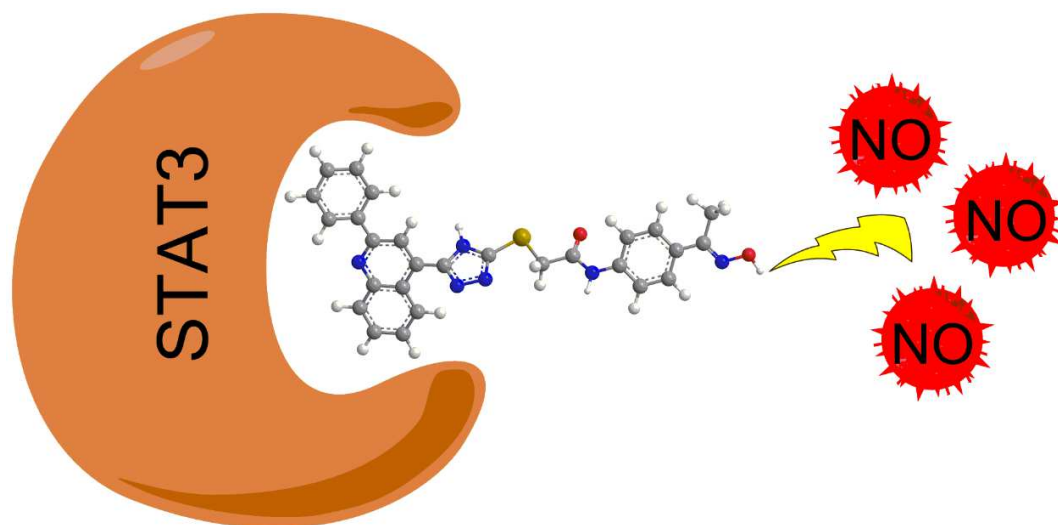
<sup>#</sup>Contributed equally to this work.

<sup>\*</sup>Corresponding authors.

E-Mail Address: [dalia\\_abdelhameed@mu.edu.eg](mailto:dalia_abdelhameed@mu.edu.eg) (D. Abdelhamid).

E-Mail Address: [dalby@austin.utexas.edu](mailto:dalby@austin.utexas.edu) (KN. Dalby).

Graphical Abstract



Journal Pre-proof

## Abstract

Constitutive activation of STAT3 can play a vital role in the development of melanoma. STAT3-targeted therapeutics are reported to show efficacy in melanomas harboring the BRAFV600E mutant and also in vemurafenib-resistant melanomas. We designed and synthesized a series of substituted nitric oxide (NO)-releasing quinolone-1,2,4-triazole/oxime hybrids, hypothesizing that the introduction of a STAT3 binding scaffold would augment their cytotoxicity. All the hybrids tested showed a similar level of *in vitro* NO production. **7b** and **7c** exhibited direct binding to the STAT3-SH domain with IC<sub>50</sub>s of 320 and 250 nM. Also, they abrogated STAT3 tyrosine phosphorylation in several cancer cell lines, including the A375 melanoma cell line that carries the BRAFV600E mutation. At the same time, they did not affect the phosphorylation of upstream kinases or other STAT isoforms. **7c** inhibited STAT3 nuclear translocation in mouse embryonic fibroblast while **7b** and **7c** inhibited STAT3 DNA-binding activity in the A375 cell line. Their anti-proliferating activity is attributed to their ability to trigger the production of reactive oxygen species and induce G1 cell cycle arrest in the A375 cell line. Interestingly, **7b** and **7c** showed robust cell growth suppression and apoptosis induction in two pairs of BRAF inhibitor-naïve (-S) and resistant (-R) melanoma cell lines containing a BRAF V600E mutation. Surprisingly, MEL1617-R cells that are known to be more resistance to MEK inhibition by GSK1120212 than MEL1617-S cells exhibit a comparable response to **7b** and **7c**.

## Keywords

Quinolines; Triazoles; STAT3; NO donors; Melanoma; acquired resistance to BRAF-inhibition; BRAF V600E mutant.

## Introduction

Malignant melanoma is an aggressive form of skin cancer that arises from the unregulated proliferation of melanocytes.<sup>1, 2</sup> Despite its low incidence (only 4 percent of all dermatologic cancers), it is responsible for 80 percent of deaths from skin cancer and is characterized by a low survival rate. Vemurafenib is an FDA approved BRAF inhibitor used for metastatic melanoma patients, but the development of resistance to this drug represents a significant hurdle to successful treatment.<sup>3</sup> This resistance occurs through several mechanisms, which often involve the reactivation of ERK, but also includes mechanisms independent of ERK reactivation.<sup>1</sup>

Signal transducers and activators of transcription (STATs 1-4, 5a-b and 6) are a family of transcription proteins that regulate gene expression related to cellular processes, including proliferation, differentiation, angiogenesis, apoptosis, and immune response.<sup>4</sup> STAT3 is activated through cytokine (e.g. interleukins) or growth factor (e.g. EGF) binding to cell surface receptors, which results in its phosphorylation at Tyr705, followed by dimerization and translocation to the nucleus, where it binds to specific DNA sequences, and induces transcription.<sup>4, 5</sup> STAT3 possesses a secondary phosphorylation site, Ser727, whose phosphorylation is essential for maximal transcriptional activity.<sup>6</sup> In normal cells, the duration of STAT3 activation is transient, however; in cancer cells, STAT3 signaling is often constitutive.<sup>4</sup>

STAT3 may play a role in melanoma development. For example, the expression of a STAT3 dominant-negative variant, STAT3b, was found to cause inhibition of tumor growth and induce cell death in murine B16 melanoma cells.<sup>7</sup> However, while STAT3 induces growth inhibition of normal melanocytes and early-stage melanoma cells, it promotes growth of advanced melanomas<sup>8</sup> and notably, blockage of activated STAT3 in metastatic cells suppresses their

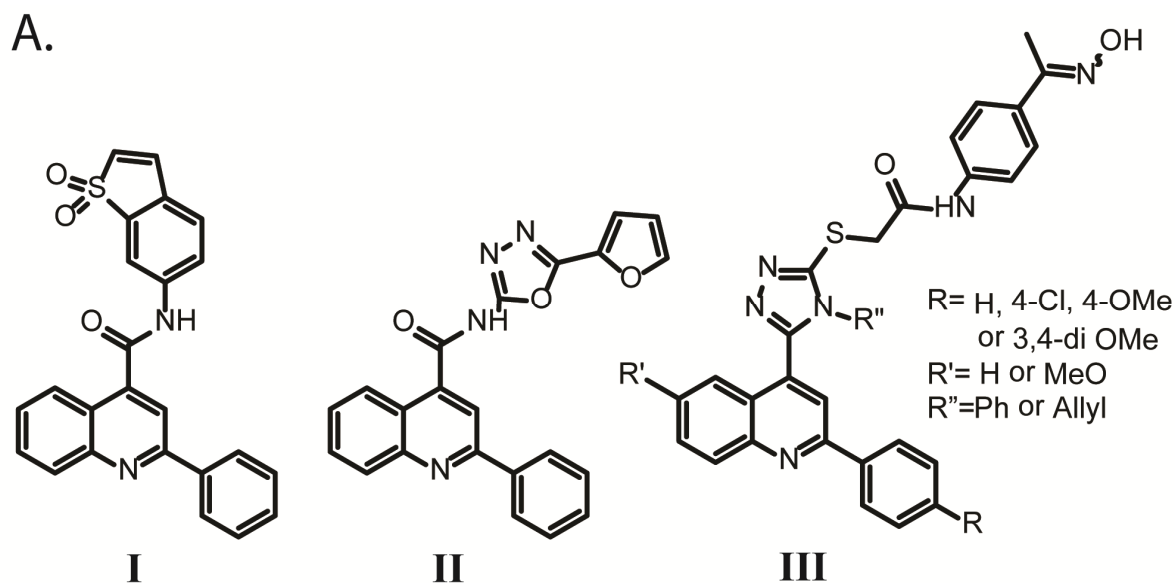
invasiveness, and inhibits tumor growth and metastasis in nude mice.<sup>9</sup> Mutant BRAF is known as a significant driver of proliferation, metastasis, and survival of almost 50% of melanomas. Interestingly, Becker et al<sup>10</sup> report that phosphorylation of STAT3 in melanoma is enhanced by the existence of the BRAF (V600E) mutant. STAT3 activation leads to phosphorylation and stabilization of the anti-apoptotic protein Mcl-1 that drives melanoma survival and chemoresistance.

Several small-molecule inhibitors of BRAF were developed a few years ago, including vemurafenib and dabrafenib. Unfortunately, these inhibitors generally exhibit a temporary response, in patients with BRAF-mutant melanomas.<sup>11-14</sup> Notarangelo et al<sup>15</sup> reported that the IL6/STAT3 axis is one of the primary regulators of acquired resistance to a BRAF inhibitor in BRAF mutant thyroid carcinoma cells. Exposure of cells to PLX4032 (BRAF inhibitor) triggered reprogramming of the expression of several genes, including JAK/STAT3. Interestingly, the dual targeting of BRAF and STAT3 in these cells showed an enhanced response with minimal acquired resistance to the BRAF inhibition.<sup>15</sup> Moreover, another recent report suggested that targeting the STAT3-paired box homeotic gene 3 (PAX3)-signaling pathway could overcome acquired resistance to Vemurafenib and it was suggested that combination-targeted therapies could provide a plausible solution to overcome this resistance in melanoma patients.<sup>3</sup>

Over the past years, many peptidic and non-peptidic STAT3 inhibitors have been discovered to inhibit STAT3 phosphorylation and dimerization. However, to date, none of these have been marketed due to either lack of efficacy (e.g., STA-21, LLL-3, curcumin, and their analogs) or unusual side effect profiles (e.g., OPB51602 and OPB-31121).<sup>16-19</sup> A new generation of OPB compounds are currently being evaluated in early phase clinical trials, and so far show improved toxicity profiles.<sup>19</sup>

Here we report the design and synthesis of novel anticancer hybrids comprised of a quinolone, a triazole, and an oxime moiety (nitric oxide donor). Quinoline-containing scaffolds are well-recognized as chemotherapeutic anticancer agents.<sup>20</sup> Many triazoles and bistriazoles possess pharmacological activities (e.g., antibacterial, antifungal, anti-inflammatory, and anticancer)<sup>21</sup> and several triazoles have been incorporated into clinically approved drugs.<sup>22</sup> These heterocycles possess significant dipole moments that are capable of forming favorable hydrogen bonds to biomolecules.<sup>23</sup> Recently, triazoles have been reported to suppress STAT3 phosphorylation, which further increases their chemotherapeutic potential.<sup>22, 24</sup> Several reports (reviewed recently,<sup>25</sup>) have shown that exposure to elevated concentrations of NO can suppress cancer progression.

Compounds **I** and **II** (Figure 1A) were previously reported to inhibit STAT3 SH2 domains.<sup>26, 27</sup> Compound **I** suppresses cell progression and induces apoptosis in breast and pancreatic cancer cell lines. It inhibits the proliferation of MDA-MB-231 and MCF7 cell lines with IC<sub>50</sub>s of 0.1 and 0.29  $\mu$ M, respectively. Treatment of MDA-MB-231 cells with 5  $\mu$ M of compound **I** inhibits STAT3 transcription by 65%, compared to a non-treated control.<sup>26</sup> Compound **II** inhibits STAT3 transcriptional activity in HeLa cells with an IC<sub>50</sub> of 74  $\mu$ M.<sup>27</sup> We docked these compounds onto the STAT3 SH2 domain (PDB code: 1BG1) using AutoDock Vina<sup>26, 28, 29</sup> and found that the 2-phenyl group on the quinoline ring fits effectively into a hydrophobic cleft near to Ile634. In this current study, a newly designed scaffold (**III**) (Figure 1A), comprised of a quinolone and triazole motif, was selected based on its similarity to compounds **I** and **II** and was combined with an oxime-based NO donor to augment its STAT3 inhibitory properties with the cytotoxic release of nitric oxide.



B.

Comparison of inhibitory activity towards two normal cell lines and A375 melanoma cell growth.

Cell Line	Comp 7b	Comp 7c	Comp 7g	Compound II
HFF-1	54.4±3.7	199.5±11	No inhibition	72.2±1.3
MCF10A	100.0±7	92.9±7.3	No inhibition	33.4±1.7
A375	7.7±1.3	1.9±1.5	>100	16.2±1.6

Values represent Growth Inhibition  $IC_{50} \pm$  Standard Error (n=3) in  $\mu$ M

C.

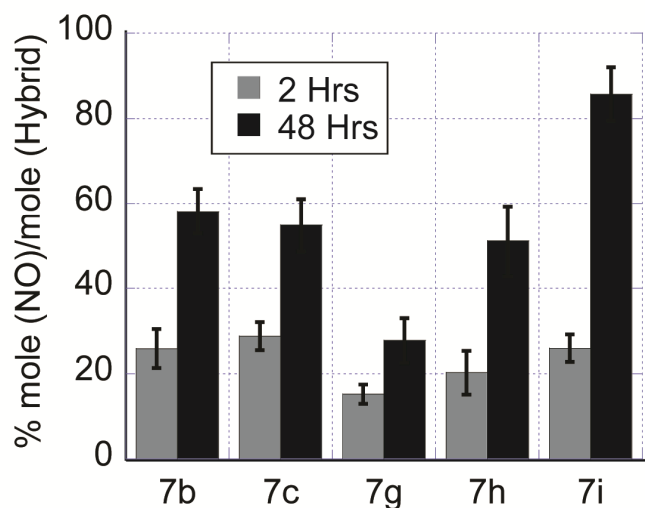


**Figure 1.** (A) Structures of compounds I, II, and III. (B) This table represents the inhibitory activity of three hybrids 7b, 7c, and 7g, as well as the lead compound II towards the growth of two normal cell lines MCF10A (human breast epithelial cell line) and HFF1 (Human foreskin fibroblasts) in comparison to A375 melanoma cell line. (C) Percentage of NO released from

compounds **7b**, **7c**, **7g**, **7h**, and **7i** in phosphate buffer (pH 7.4) after 2 and 48 hours using a modified Griess colorimetric method (The methods section).

Here we set out to develop a novel series of hybrids based on scaffold **III** (Figure 1A) to identify promising anticancer candidates with the potential to overcome BRAF-inhibitor acquired resistance in melanoma cells. The structural variability of the hybrid compounds was obtained by using different substituents (**R**, **R'**) on C-2 of the phenyl ring and C-6 of the quinoline ring, respectively. Compounds were chemically synthesized, and then their ability to release NO, bind STAT3, suppress STAT3 activity and inhibit cancer cell growth were evaluated in several cancer cell lines, including both SB-590885-sensitive and SB-590885-resistant melanoma cell lines.

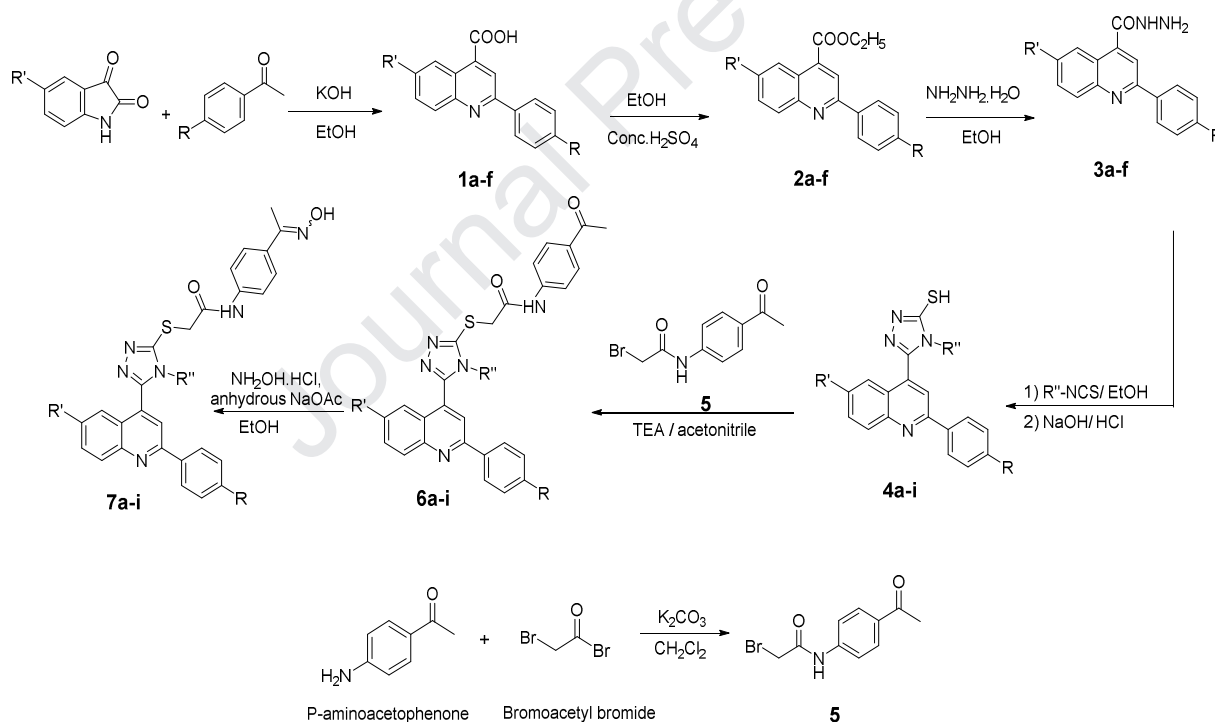
## 2. Results and discussion

### 2.1. Chemistry

The reaction sequence employed to synthesize the target compounds is outlined in **Scheme 1**. The initial 2-(substituted phenyl) quinoline-4-carboxylic acids **1a-f** were obtained by reacting 5-methoxyisatin or isatin with an appropriate acetophenone. These acids were then refluxed with absolute ethanol in the presence of conc. H<sub>2</sub>SO<sub>4</sub> to afford the corresponding esters **2a-f**. Afterward, the ethyl esters **2a-f** were converted to carbohydrazide derivatives **3a-f** via reaction with hydrazine monohydrate. The formation of these intermediates was confirmed by their reported melting points. The carbohydrazides were heated at reflux with allyl or phenyl isothiocyanate in ethanol. This was followed by the addition of 2N NaOH, then acidification with conc. HCl, affording 1,2,4-triazole-3-thiol derivatives **4a-i**. The chemical identity of the synthesized compounds was confirmed by <sup>1</sup>H-NMR and <sup>13</sup>C-NMR spectra. Compound **5** was

prepared through acetylation of p-aminoacetophenone with bromoacetyl bromide in the presence of potassium carbonate. Afterward, compound **5** was then coupled with the 1,2,4-triazole derivatives **4a-i** in acetonitrile in the presence of triethylamine affording the nine ketone intermediates **6a-i**. The final nine NO-donating oxime derivatives **7a-i** were prepared by reacting compounds **6a-i** with hydroxylamine hydrochloride in the presence of anhydrous sodium acetate.

	<b>1a</b>	<b>1b</b>	<b>1c</b>	<b>1d</b>	<b>1e</b>	<b>1f</b>	<b>4a</b>	<b>4b</b>	<b>4c</b>	<b>4d</b>	<b>4e</b>	<b>4f</b>	<b>4g</b>	<b>4h</b>	<b>4i</b>
R	H	4-Cl	4-OMe	4-Cl	4-OMe	3,4-di OMe	H	H	4-Cl	4-Cl	4-OMe	4-OMe	4-Cl	4-OMe	3/4-OMe
R'	H	H	H	OMe	OMe	OMe	H	H	H	H	H	H	OMe	OMe	OMe
R''	-	-	-	-	-	-	Ph	Allyl	Allyl	Ph	Ph	Allyl	Ph	Ph	Ph
							<b>7a</b>	<b>7b</b>	<b>7c</b>	<b>7d</b>	<b>7e</b>	<b>7f</b>	<b>7g</b>	<b>7h</b>	<b>7i</b>
R							H	H	4-Cl	4-Cl	4-OMe	4-OMe	4-Cl	4-OMe	3/4-OMe
R'							H	H	H	H	H	H	OMe	OMe	OMe
R''							Ph	Allyl	Allyl	Ph	Ph	Allyl	Ph	Ph	Ph



**Scheme1.** Synthesis of **6a-i** and the corresponding oximes **7a-i**.

## 2.2 Biology

### 2.2.1 Screening of anticancer activity and SAR analysis

The overexpression or constitutive activation of STAT3 has been identified in almost 70% of solid and hematological human tumors, and its constitutive activation correlates with poor survival.<sup>4</sup> Accordingly, the anticancer activity of the hybrids developed in this study was evaluated in several cancer cell lines. A total of eighteen compounds were synthesized: 9 ketones and 9 oximes. Eleven compounds, **6a**, **6e**, **6g**, and **7b-i**, were selected by the National Cancer Institute (NCI) for anticancer screening according to the protocol of the Drug Evaluation Branch of the National Cancer Institute, Bethesda, USA. *In vitro* anticancer screening was carried out in 60 cell lines of nine different cancer cell types; ovarian, renal, prostate, leukemia, melanoma, lung, colon, CNS, and breast cancers. Compounds were added at a single concentration of 10  $\mu$ M for 48 h. Endpoint determinations were made using a protein-binding dye, sulforhodamine B (SRB), that enables quantification of the number of cells in each well. Results for each compound were reported as the growth percent inhibition of the treated cells, which are evaluated spectrophotometrically and compared to that of the untreated control cells.

Oximes **7b-i** showed promising anticancer activity varying from moderate to significant growth inhibition against most of the 60 cancer cell lines. **7b**, **7c**, and **7f** were the most effective hybrids against the cell lines shown in Table S1. Compound **7b** showed inhibitory activity against leukemia (MOLT-4 and CCRF-CEM), melanoma (LOX IMVI and UACC-62), ovarian (IGROV1), and breast (MCF7 and T-47D) cancer cell lines with percent growth inhibition in the range of 76-100%. Compound **7c** was effective against leukemia, non-small cell lung, and colon cancer cell lines. Furthermore, it incurred significant growth inhibition, with complete cell death in leukemia (MOLT-4), melanoma (LOX IMVI), ovarian (IGROVI) and renal (UO-31) cell lines (Table S1). Compound **7f** caused complete cell death against both leukemia (HL-60 (TB)) and

breast (T-47D) cancer cell lines and induced potent growth inhibition (81-98%) against the leukemia cell lines; (CCRF-CEM, K-562, MOLT-4, and RPMI-8226). Compound **7f** also inhibited the growth of the A549/ATCC and NCI/H522 non-small cell lung cancer cell lines as well as the colon cancer cell line, COLO 205, and several other cell lines (Table S1).

We also assessed three of the hybrids (**7b**, **7c** and **7g**) and the lead compound II (STX-0119, structure shown in Figure 1A and purchased from Key Organics Limited) for their ability to inhibit the growth of the non-cancer cell lines, MCF10A (human breast epithelial cell line) and HFF1 (Human foreskin fibroblasts). The data shown in Figure 1B reveal a relative resistance of these cells to the hybrids when compared to the melanoma cell lines A375 (Figure 1B). For example, **7c** inhibited cellular growth of HFF1 and MCF10A with  $IC_{50}$  values of  $200 \pm 11$  and  $93 \pm 7.3$   $\mu$ M compared to an  $IC_{50}$  of  $1.9 \pm 1.5$   $\mu$ M for the A375 cells.

For most cell lines, compound **7c** was the most potent of the compounds tested. For example, against the A375 melanoma cell line, it exhibited a growth inhibition  $IC_{50}$  of  $1.9 \pm 1.5$   $\mu$ M, Figure 1B. **7c** is characterized by the presence of an electron-withdrawing *p*-chlorophenyl group as well as *N*-4 allyl moiety. Absence of the chloro substituent in compound **7b** decreased its ability to inhibit the growth of several NCI cell lines, including the A375 cell line that showed a growth inhibition  $IC_{50}$  of  $7.7 \pm 1.3$   $\mu$ M (Figure 1B). Replacement of the *N*-4 allyl group of compound **7c** with a bulky phenyl ring completely diminished the activity in compound **7d**. Also, replacement of the chloro group with an electron-donating methoxy group (e.g., **7f**), moderately enhanced the activity compared to **7c** (Table S1). The activity of **7f** sharply declined upon replacement of the *N*-4 allyl moiety with a phenyl ring (**7e**). Compounds **7h** and **7i**, showed an average growth inhibition percent, with the presence of electron-donating methoxy and dimethoxy substituents decreasing the overall anticancer activity against most of the cell lines, except for the melanoma LOX IMVI cell line. In conclusion, compounds with a ketonic

group showed very weakly, or no activity against most of the cancer cell lines tested (compounds **6a**, **6e**, and **6g**). While the oximes (compounds **7b-i**), exhibited an increase in the activity against most of the cancer cell lines tested, consistent with a role for NO in the activity. Also, compounds with a small substituent (allyl group) on the triazole ring exhibited better activity than those with large substituent (phenyl group) (compound **7c** versus **7d**).

### 2.2.2 NO-releasing hybrids

In 2008, Thomas et al<sup>30</sup> investigated the effect of nitric oxide (NO) on MCF7 cells. While lower levels of NO promoted cell survival and proliferation, higher levels of NO (*c.a.* 400 nM) induced apoptosis, cell cycle arrest, and cytotoxicity. In order to determine if our hybrids can produce the high level of nitric oxide, sufficient to induce cytotoxicity, the ability of each hybrid to donate NO was estimated using the modified Griess colorimetric method (Figure 1C). Five hybrids (**7b**, **7c**, **7g**, **7h**, and **7i**) were tested after 2 and 48 hours of incubation at room temperature in phosphate buffer (pH 7.4) and each showed a comparable ability to release NO in phosphate buffer corresponding to 15-28% (mole NO/mole compound) after 2 hours and increased to 30-85% (mole NO/mole compound) after 48 hours (Figure 1C).

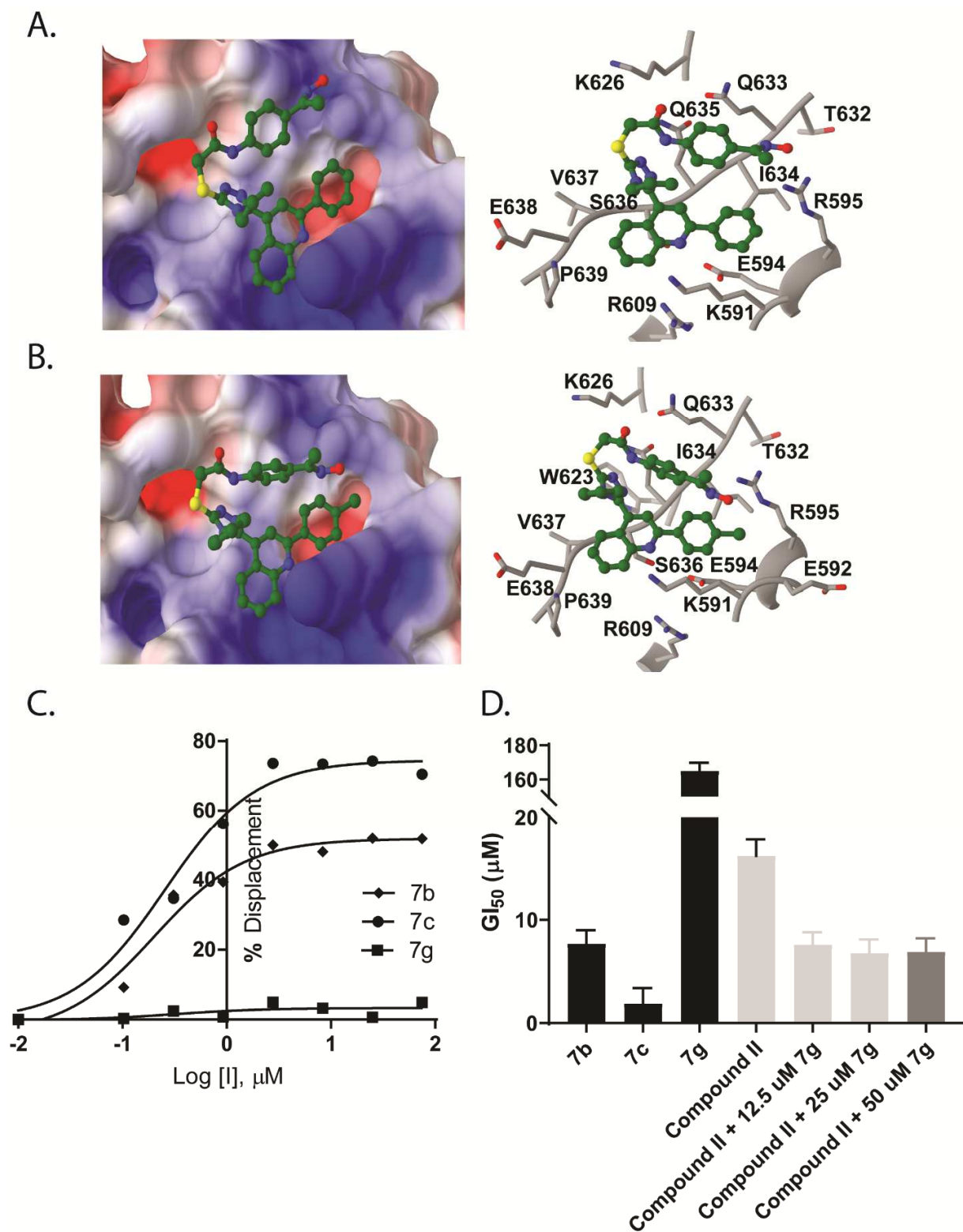


**Figure 2.** (A-B) Predicted conformations of compounds **7b** and **7c** in the STAT3-SH2 domain (PDB ID: 1BG1) from docking (AutoDock 4.2). (A-left, B-left) Represents the electrostatic

potential surface for the binding pocket of the STAT3-SH2 domain with compounds **7b** and **7c**. The electrostatic potential varied from  $-5K_B T/e$  to  $+5K_B T/e$  from red to blue. **(A-right, B-right)** Represents the trajectories for compounds **7b** and **7c** binding to the STAT3-SH2 domain. STAT3-SH2 residues engaging the ligand are explicitly shown in grey stick representation. The ligands are shown green ball and sticks. **(C)** The effect of **7c**, **7b**, and **7g** in a recombinant STAT3 displacement assay using a FAM labeled 5-GpYLPQTV-NH2 peptide; Data shows the average from two independent experiments. **(D)** The ability of **7b**, **7c**, **7g**, compound **II**, or different combinations of compounds **II** and **7g** to inhibit proliferation of A375 melanoma cell line. Cells were treated with different doses of each inhibitor or different doses of compound **II** in the presence of a fixed concentration of **7g** (12.5, 25, or 50  $\mu$ M) for 48 hours, and viability was determined using MTS assay (Promega). The Y-axis represents  $GI_{50}$  (The concentration that resulted in 50% Growth inhibition) for each inhibitor or each combination. **7b**, **7c**, **7g**, and compound **II** bars represent the values shown in Figure 1B. Data show the average from three independent experiments.

**2.2.3 Direct binding to the STAT3 SH2 domain** - A binding mode for the binding of **7b** and **7c** to the STAT3-SH2 domain was predicted using molecular docking (Figure 2A and 2B respectively). Docking calculations were carried using AutoDock4.21 (method section) based on the X-ray structure of the STAT3 $\beta$  homodimer (PDB ID: 1BG15)<sup>28</sup>. The docking scores for compounds **7b** and **7c** were  $-10.37$  and  $-9.89$  kcal mol<sup>-1</sup>, respectively. Therefore, compound **7b** can form a slightly more energetically favorable interaction with STAT3-SH2 than **7c**. As shown in Figure 2A and 2B, the 2-phenyl rings of **7b** and **7c** are inserted into the hydrophobic cleft formed by I634, V637, P639 and T632. The OH group in the NO of **7b** and **7c** is also stabilized via hydrogen bonds to the side chains of R595.

To further investigate the direct binding of the new compounds with the SH2 domain of STAT3, we developed a displacement assay to estimate the ability of these compounds to displace the 5-FAM-GpYLPQTV-NH2 peptide<sup>31</sup> from recombinant GST-STAT3 (Figure 2C). **7b** and **7c** showed robust ability to displace the phospho-peptide in a dose-dependent manner

(IC<sub>50</sub>s 0.32±0.19 and 0.25±0.13μM, respectively) while **7g** did not show any tendency to bind the STAT3 SH2 domain as it was not able to entirely displace the peptide from the surface of GST-STAT3 (Figure 2C).

It is noticeable in the NCI screening results shown in Table S1 that despite the limited growth inhibition caused by the two oximes **7e** and **7g**, their corresponding ketones **6e** and **6g** showed no growth inhibition in comparison (compare **7g** and **6g** in Table S1), supporting the notion that the nitric oxide (NO) donating ability of **7e** and **7g** contributes to the inhibition of cancer cell proliferation.<sup>25</sup> These results directly correlate with the ability of **7b** and **7c** to inhibit cancer cell proliferation by both targeting the STAT3 SH2 domain and releasing NO while the mild cytotoxicity observed for **7g** was likely due to its ability to produce NO (Table S1 and Figure 1C).

In order to assess the value of combining dual functions into single hybrid molecules, an experiment was conducted where the cytotoxicity of compounds **II** (Lead STAT3 inhibitor, Figure 1A), compounds **7b** and **7c** (STAT3 inhibitor with NO-releasing moiety) and compound **7g** (NO-releasing compound) were compared, in addition to different combinations of compounds **II** and **7g** against A375 melanoma cell line. The results shown in Figure 2D revealed higher potency of **7b** and **7c** hybrids towards the A375 cell line compared to compound **II** (IC<sub>50</sub>s of 7.7, 1.9, and 16.2 μM, respectively) or compound **7g** alone. Addition of the NO-releasing **7g** to compound **II** exhibited an additive cytotoxic effect where compound **II** IC<sub>50</sub> towards A375 cells decreased from 16.2±1.6 to 6.8±1.3 μM in the presence of 12.5 μM **7g**, which is similar to the IC<sub>50</sub> of **7b** against the same cell line (Figure 2D). The additive effects observed between **7g** and compound **II** validates the design of these hybrids where the cytotoxicity of the released NO enhances the cytotoxicity caused by STAT3 pathway inhibition.

#### 2.2.4 The designed hybrids are selective STAT3 inhibitors *in cancer cells*

In order to rationalize the anticancer activity of these hybrids and to understand if it correlates with their ability to inhibit STAT3 and/or to donate NO, it was essential to study their molecular mechanism of action in more detail. Compounds **7b** and **7c** exhibited a toxic effect on most of the cancer cell lines tested (Table S1). This significant cytotoxic activity may be attributed to their ability to bind and inhibit STAT3 activity,<sup>32</sup> besides their ability to release nitric oxide.

**7b and 7c inhibited STAT3 tyrosine phosphorylation in different cancer cell lines without affecting the upstream kinases** - To examine the ability of the new compounds to inhibit STAT3 signaling, different cancer cell lines, including the glioblastoma U87-MG, the breast cancer cell line MDA-MB-468, the pancreatic carcinoma cell line Miapaca-2 and the non-small cell lung cancer cell lines NCI-H157 and A549 were incubated with 25  $\mu$ M of **7b** overnight, before lysing the cells and immunoblotting. The melanoma cell line A375 that expresses the BRAF V600E mutant was exposed to different doses of **7b** and **7c** (0, 5, 10, and 25  $\mu$ M) following the same protocol. As shown in Figure 3A and 3B, **7b** exhibited a robust inhibition of STAT3 phosphorylation at Y705 and S727 in all the cell lines tested with enhanced potency in A375 cells. **7c** inhibited the phosphorylation of STAT3 with lower potency in A375 cell lines, compared to **7b** (5-10  $\mu$ M of **7b** or 10-25  $\mu$ M **7c** were enough to inhibit STAT3 phosphorylation) (Figure 3B). Interestingly, **7b** and **7c** did not show any effect on the phosphorylation of the upstream tyrosine kinases (JAK2 and Src) in all the cell lines tested or ERK1/2 in A375 cell line (Figure 3A and 3B).

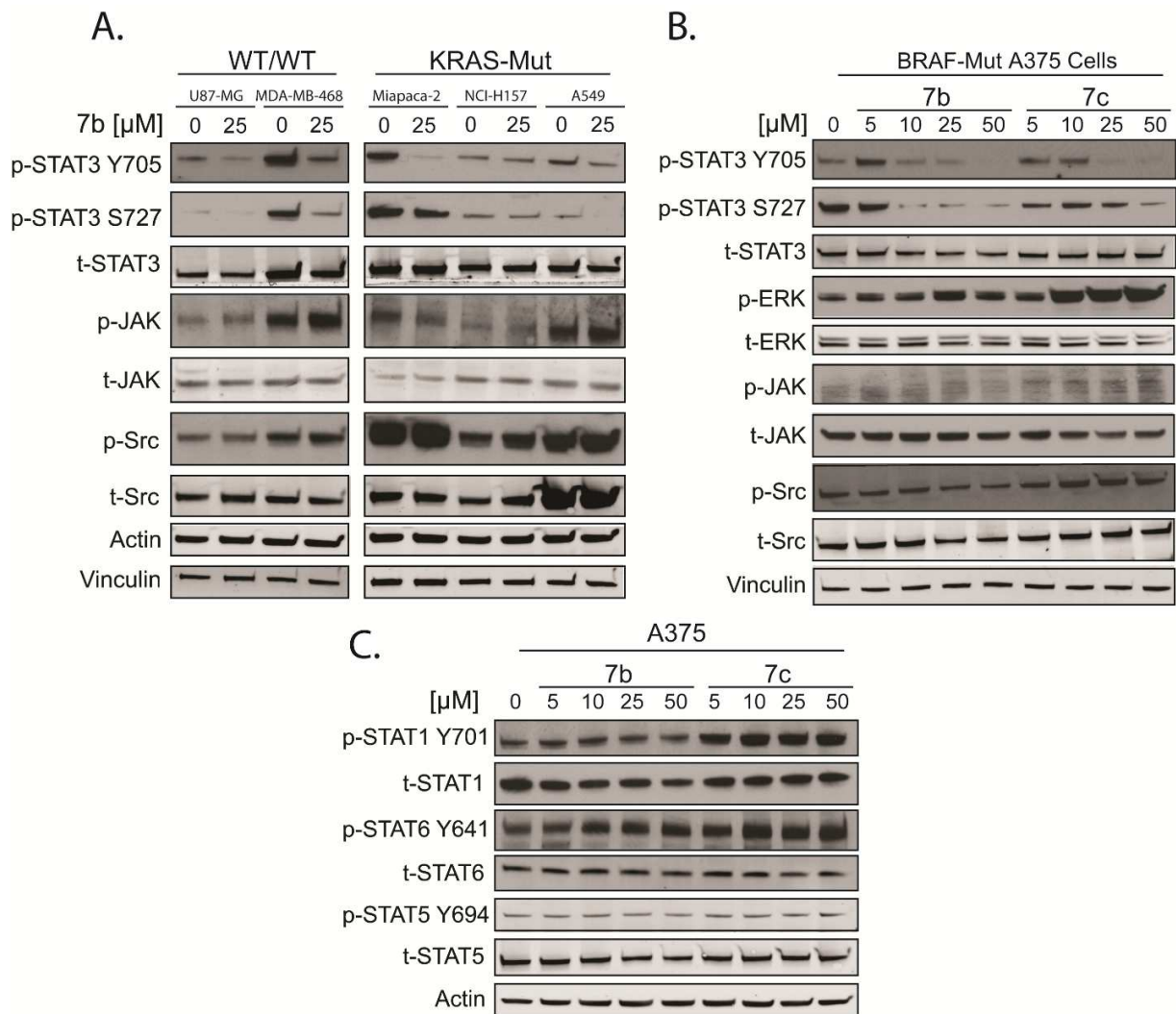


**Figure 3** (A) The ability of **7b** to suppress STAT3 phosphorylation in three KRAS mutant and two wild-type cancer cell lines without affecting the upstream tyrosine kinases JAK2 and Src. (B) **7b** and **7c** inhibited STAT3 phosphorylation in the RAF mutant cell line A375 at both Y705 and S727 without affecting the phosphorylation of the STAT-3 activators Src and JAK2 and the phosphorylation of the STAT-3 regulated protein ERK. (C) **7b** and **7c** inhibited STAT3 phosphorylation without affecting the phosphorylation of STAT1 at Y701, STAT5 at Y694, and STAT6 at Y641. In all these experiments, A375 cells were treated with different doses of each inhibitor for 20 hours. Protein expression and phosphorylation were assessed using western blotting, actin, vinculin, or both were employed as loading controls.

**The selectivity of 7b and 7c towards STAT3 isoform** - We showed earlier that **7b** and **7c** directly bind the STAT3 SH2 domain and inhibit STAT3 phosphorylation in A375 cell lines

without affecting upstream kinases (Figure 2C and 3B). In this experiment, we investigated the selectivity towards other STAT isoforms, including STAT1, STAT5, and STAT6 (Figure 3C). Immunoblots shown in Figure 3C for A375 cells incubated with different doses of **7b** or **7c** overnight suggest that neither inhibitor inhibits the phosphorylation of STAT1 at Y701, STAT5 at Y694 nor STAT6 at Y641 even at high inhibitor concentrations (50  $\mu$ M). This suggests that **7b** and **7c** are selective STAT3 inhibitors in the BRAF V600E mutant A375 melanoma cell line.

**7c inhibited STAT3 nuclear translocation** - STAT3 immunostaining in mouse embryonic fibroblasts (MEF) that were maintained overnight in serum-free media, revealed the existence of most of the non-phosphorylated STAT3 in the cytoplasm. Induction of STAT3 phosphorylation by EGF for 30 minutes before staining triggered the migration of around 60-70% of the STAT3 molecules to the nucleus (Figure 4A). These observations are comparable to previous reports.<sup>33, 34</sup> Cells that were incubated in serum-free media containing different doses of **7c** for the same time abrogated the EGF response and prevented the migration of STAT3 to the nucleus in a dose-dependent manner (Figure 4A). This suggests that **7c** can target STAT3 in MEFs to inhibit its phosphorylation and nuclear translocation.

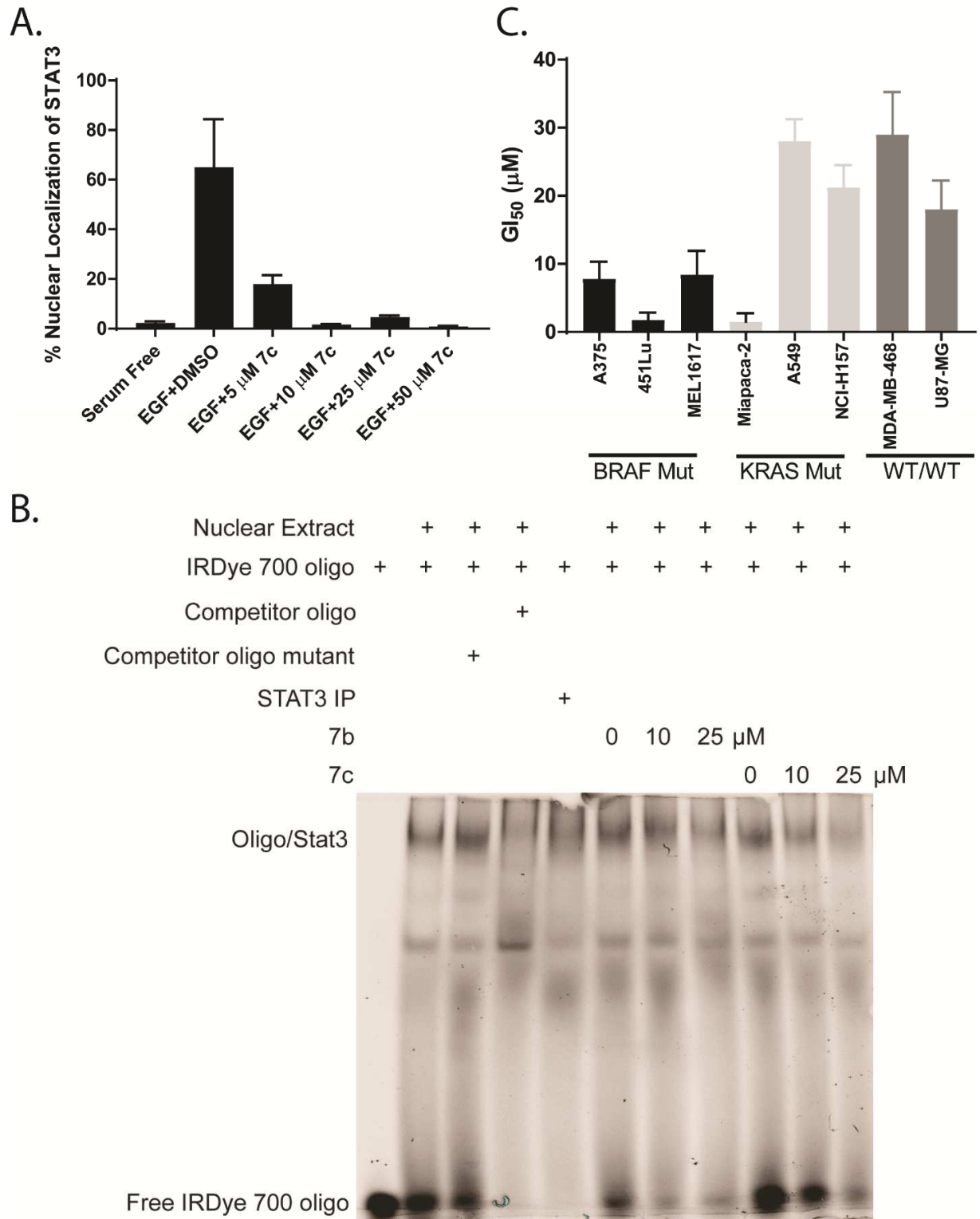


**Figure 4 (A)** **7c** inhibited EGF triggered nuclear translocation of STAT3 in MEF cells (Mouse Embryonic Fibroblasts), in a dose-dependent manner; Data show the average from three independent experiments; **(B)** Electrophoretic mobility shift assay (EMSA) were employed to examine the effect of **7b** and **7c** on the DNA binding activity of STAT3 in A375 cell line using IRDye 700-labeled DNA oligo (LI-COR Biosciences), competitor oligo and oligo mutant (Santa Cruz Biotechnologies) were employed as positive and negative controls, respectively. STAT3-IP represents nuclear extract of cells where STAT3 was immune-precipitated; **(C)** **7b** ability to inhibit proliferation of various BRAF/KRAS mutant and wild-type cancer cell lines. Cells were treated with different doses of **7c** for 48 hours, and viability was determined using MTS assay (Promega). The Y-axis represents **7c** GI50 (The concentration that resulted in 50% Growth inhibition) versus the cancer cell line on the X-axis. Data show the average from three independent experiments;

**7b and 7c inhibit the DNA-binding activity of STAT3** - To examine the ability of **7b** and **7c** to inhibit the DNA-binding activity of STAT3 in the A375 melanoma cell line, EMSA (Electrophoretic Mobility Shift Assay) was performed using an IRDye® 700 STAT3 consensus oligonucleotide and nuclear extract of A375 cells following the manufacture protocol (methods section).<sup>35-37</sup> As shown in Figure 4B, STAT3 binding to the IRDY 700 oligo was confirmed using a competitive oligo and mutant. As a further control, STAT3 was immunoprecipitated from cells. Cells treated overnight with different doses of **7b** or **7c** before nuclear extraction showed significant dose-dependent inhibition of the DNA binding activity of STAT3 (Figure 4B).

The data presented in this section suggest the hybrids specifically target the STAT3 isoform in cancer cells (Figure 2A, 2B and 2C), to suppress its phosphorylation (Figure 3A and 3B) and nuclear translocation (Figure 4A), leading to inhibition of its dimerization and its ability to bind DNA in the nucleus (Figure 4B). DNA binding is required to trigger STAT3 transcription activity.

### 2.2.5 Sensitivity of mutant KRAS or BRAF-expressing cells towards STAT3 inhibition by **7b**

It was recently reported that the survival and chemoresistance of melanoma harboring the BRAF (V600E) mutant could be attributed to enhanced STAT3 activation.<sup>10</sup> At the same time, a recent report by Gough et al<sup>38</sup> investigated the role of STAT3 in a murine K-Ras G12D mutant-dependent hematopoietic neoplasia. Inhibition of STAT3 phosphorylation at S727 by point mutation caused a substantial delay in the onset of the disease. This suggested the importance of mitochondrial STAT3 phosphorylation at S727 as a mediator of K-RAS induced neoplastic hematopoietic cell growth. From these observations, we hypothesized that our new inhibitors might show enhanced cytotoxic activities in cells expressing BRAF or KRAS mutants compared to cells expressing their WT forms.

Figure 4C shows the effect of **7b** on inhibiting the proliferation of different cancer cell lines including the glioblastoma and breast cancer cell lines (U87-MG and MDA-MB-468) that express wild type forms of BRAF and KRAS, the pancreatic carcinoma cell line Miapaca-2 and the non-small cell lung cancer cell lines NCI-H157 and A549 that express mutated form of KRAS as well as the BRAF V600E mutant melanoma cell lines A375, 451 Lu and MEL 1617. Interestingly, cells expressing the BRAF-mutant are more sensitive to **7b** compared to cells expressing wild type BRAF and KRAS, as well as mutant KRAS (Figure 4C), and in all cases, sensitivity appears to correlate with inhibition of STAT3 phosphorylation at both Y705 and S727 (Figure 3A, 3B and 7A).

### 2.2.5 Sensitivity of mutant KRAS or BRAF-expressing cells towards STAT3 inhibition by **7b**

It was reported recently that the survival and chemoresistance of melanoma harboring the BRAF (V600E) mutant could be attributed to enhanced STAT3 activation.<sup>10</sup> At the same time, a recent report by Gough et al<sup>38</sup> investigated the role of STAT3 in a murine K-Ras G12D mutant-dependent hematopoietic neoplasia. Inhibition of STAT3 phosphorylation at S727 by point mutation caused a substantial delay in the onset of the disease. This suggested the importance of mitochondrial STAT3 phosphorylation at S727 as a mediator of K-RAS induced neoplastic hematopoietic cell growth. From these observations, we hypothesized that our new inhibitors might show enhanced cytotoxic activities in cells expressing BRAF or KRAS mutants compared to cells expressing their WT forms.

Figure 4C shows the effect of **7b** on inhibiting the proliferation of different cancer cell lines including the glioblastoma and breast cancer cell lines (U87-MG and MDA-MB-468) that express wild type forms of BRAF and KRAS, the pancreatic carcinoma cell line Miapaca-2 and the non-small cell lung cancer cell lines NCI-H157 and A549 that express mutated form of KRAS as well as the BRAF V600E mutant melanoma cell lines A375, 451 Lu and MEL 1617. Interestingly, cells expressing the BRAF-mutant are more sensitive to **7b** compared to cells expressing wild type BRAF and KRAS, as well as mutant KRAS (Figure 4C), and in all cases, sensitivity appears to correlate with inhibition of STAT3 phosphorylation at both Y705 and S727 (Figure 3A, 3B and 7A).

#### **2.2.6 The mechanism of anticancer activity in the BRAF mutant A375 melanoma cell line.**

**7b and 7c inhibited A375 cell proliferation** - As the STAT3 pathway regulates cell survival and proliferation,<sup>2, 4</sup> we measured the colony formation of the BRAF<sup>V600E</sup> mutant A375 melanoma cell line following incubation with different doses of **7b** and **7c**. Dose-dependent suppression of cell proliferation was noted when measured over 10 days (Figure 5A).

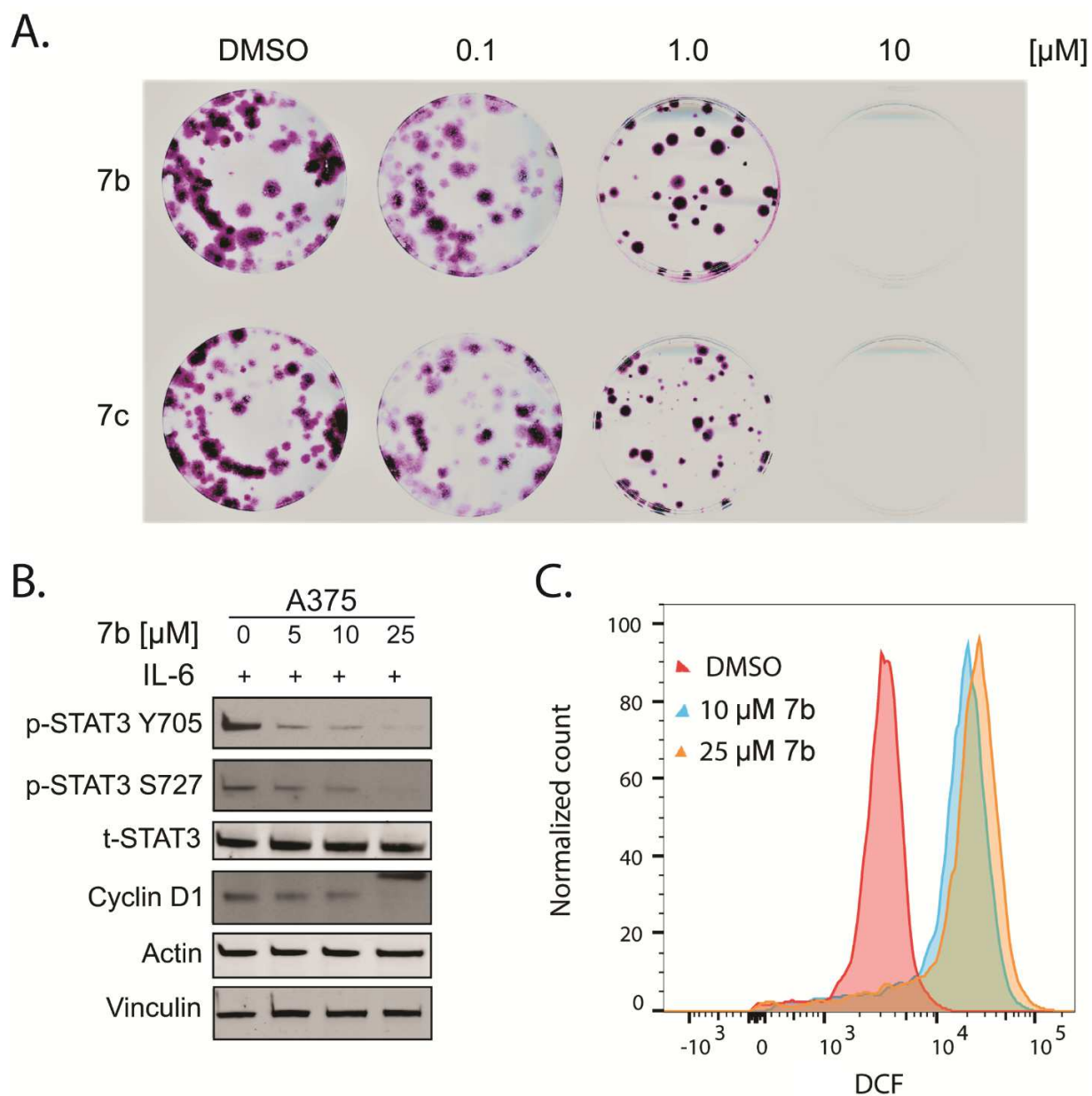


**Figure 5.** (A) **7b** and **7c** inhibited the anchorage-dependent growth of A375 cells in a dose-dependent manner. (Experiment has been repeated two times, and the results were consistent). (B) Western blot analysis showed inhibition of STAT3 phosphorylation and induction of Cyclin D1 expression in A375 cells that were treated with different doses of **7b** then induced with IL-6. (C) Compound **7b** induced ROS generation in A375 cells, ROS generation was quantified using DCFH-DA staining and analysis by flow cytometry.

**7b inhibited STAT3 cytokine-induced activation in the A375 melanoma cell line -**

Induction of STAT3 activation by cytokines such as IL-6 (interleukin-6) can be abrogated using a STAT3 inhibitor targeting the SH2 domain.<sup>35, 39</sup> To test this hypothesis in the A375 melanoma cell line, cells were incubated overnight in serum-free media containing different doses of **7b** then induced in full media containing 25 ng/mL IL-6 for 30 minutes. Cells were then harvested and lysed. The immunoblot shown in Figure 5B suggests a dose-dependent inhibition of IL-6-mediated STAT3 activation by **7b** with significant inhibition starting at a concentration of ~ 5 $\mu$ M. This was evidenced by suppression of STAT3 Y705 and S727 phosphorylation besides a dose-dependent inhibition of the expression of Cyclin D1, the STAT3 downstream protein.

**Reactive oxygen species (ROS) generation in A375 cells treated with different doses of 7b -** STAT3 acts as one of the primary regulators of the antioxidant response that eliminate cytotoxic ROS from the cell. Inhibition of STAT3 activity is expected to cause accumulation of ROS, leading to apoptosis.<sup>35</sup> ROS generation was detected in A375 cells that were incubated with different doses of **7b** overnight in full media, followed by treatment with 2',7'-dichloro-fluorescein diacetate (DCFH-DA) for 30 minutes. The amount of 2',7'-dichloro-fluorescein that corresponds to the level of ROS in the treated cells was estimated using flow cytometry. Figure 5C shows the dose-response generation of ROS in A375 cells treated with different doses of **7b**. This suggests that ROS generation may contribute to cell death.

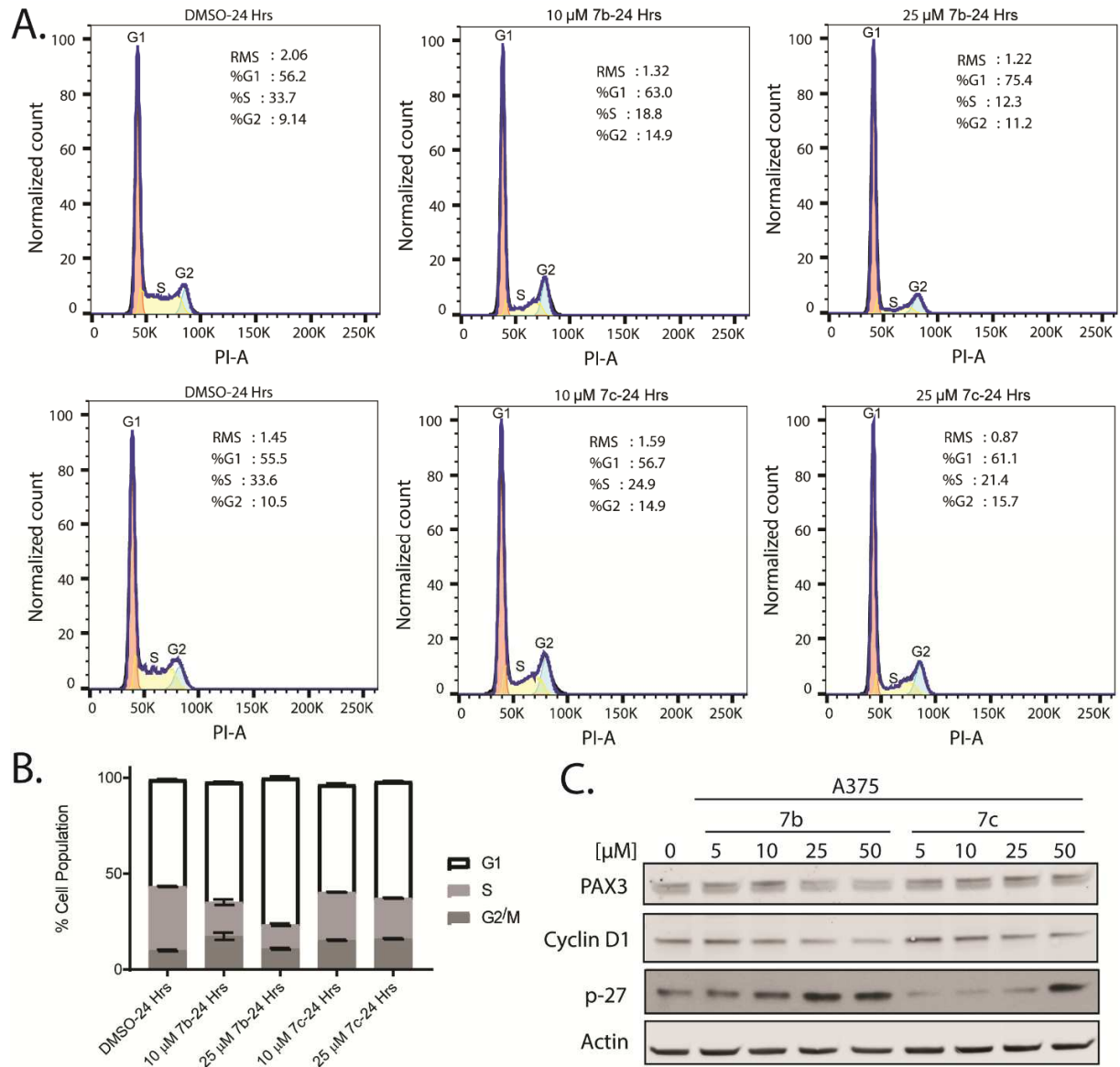


**Figure 6.** (A) FACS analysis of A375 cell nuclei stained with PI after treatment with DMSO, 10, and 25  $\mu$ M of 7b or 7c for 24 hours. The modeling feature of FlowJo V10 software was employed to analyze the PI fluorescence following a model that was reported by Watson et al<sup>40</sup>. RMS (root mean square) deviation used to evaluate the goodness of the fit. The percentage of cells modeled in each experiment was comparable. (B) Histogram showing the percentages of cells in each phase of the cell cycle (An average of three independent experiments, error bars: SEM). (C) Western blot analysis showed inhibition of PAX3 and Cyclin D1 expression and induction of p-72 expression in A375 cells that were treated for one night with different doses of 7b and 7c before lysis.

**Cell cycle arrest induction by the new hybrids in A375 cells** - Inhibition of the JAK1/2/STAT3 pathway by a small-molecule inhibitor has been reported to block the cell cycle in the G1 phase.<sup>41</sup> Cell cycle analysis of A375 cells treated with **7b** and **7c** for 24 hours revealed a dose-dependent cell cycle arrest in the G1 phase (Figure 6A and 6B). In this experiment, the G0/G1-phase fraction increased from 56.2% (DMSO treated) to 63.0% and 75.4%, at 10, 25  $\mu$ M **7b**, respectively, while increased from 55.5% (DMSO treated) to 56.7% and 61.1%, at 10, 25  $\mu$ M **7c**, respectively (Figure 6A and 6B). These observations are consistent with dose-response upregulation of p27kip1 expression and downregulation of Cyclin D1 expression that was shown by immunoblotting using cells that have been treated in the same way (Figure 6C), suggesting that inhibiting the STAT3 pathway by the new hybrids blocks cell cycle progression.

### **2.2.7 The mechanism of anticancer activity in BRAF mutant melanoma with SB-590885-acquired resistance.**

Enhanced STAT3 activation has recently been defined as one of the significant drivers of tumor acquired resistance to different treatments. For example, Lee et al. suggested that STAT3 activation promotes Erlotinib resistance in EGFR-mutant lung cancer cells.<sup>42</sup> Notarangelo et al. reported that STAT3 activation could be the primary regulator of the acquired resistance to a BRAF inhibitor in BRAF-mutant thyroid carcinoma cells.<sup>15</sup> And it was also reported that activation of STAT3 or overexpression of paired box homeotic gene 3 (PAX3) triggered resistance to vemurafenib in melanoma cell lines harboring the BRAF<sup>V600E</sup> mutation. PAX3/STAT3 downregulation or STAT3 inhibition by a small molecule suppressed the growth of vemurafenib-resistant melanoma cell lines.<sup>3</sup>

In order to investigate the ability of our new hybrids to combat the resistance to BRAF inhibitors in melanoma cell lines harboring the V600E BRAF mutant, we tested the ability of **7b**,

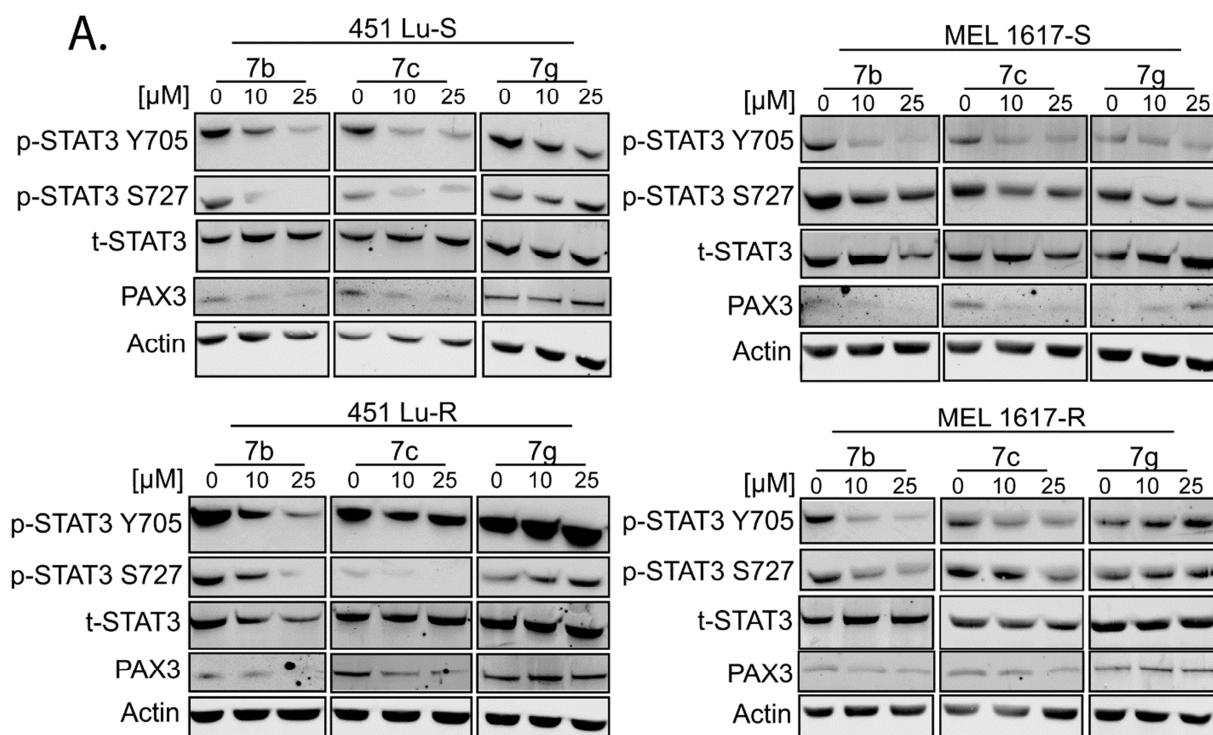
**7c, 7g, 7h** and **7i** to inhibit STAT3 activity and overcome the acquired resistance of two different melanoma cell lines to a BRAF inhibitor. The previously reported<sup>43</sup> SB-590885-resistant cell lines 451 Lu-R and MEL 1617-R, bearing the BRAF<sup>V600E</sup> mutant, were obtained by treatment with increasing concentrations of the BRAF inhibitor SB-590885. These resistant cell lines were reported to exhibit cross-resistance to other specific BRAF inhibitors including PLX4720.<sup>43</sup>

**7b and 7c inhibited STAT3/PAX feedback activation in melanoma cell lines resistant to BRAF inhibitor** - To investigate the ability of the compounds to inhibit the STAT3 pathway in resistant melanoma, we examined the effect of the inhibitors on STAT3 phosphorylation and the expression of its downstream target PAX3 in the four melanoma cell lines. Each cell line was treated with two different doses of each inhibitor (10 and 25  $\mu$ M) for 12 hours and the expression levels of STAT3 phosphorylated on Ser727 (Ser-STAT3), Tyr705 (Tyr-STAT3), total STAT3 (STAT3), total PAX3 and actin were determined and compared to a DMSO control. Figure 7A showed the ability of **7b** and **7c** to inhibit STAT3 phosphorylation and PAX3 expression in a dose-dependent manner in both SB-590885-sensitive and SB-590885-resistant 451 Lu cell lines, however the less active compounds **7g**, **7h**, and **7i** showed either limited or no ability to inhibit the STAT3 pathway in the cell lines tested (**7h** and **7i** data not shown). This suggests a correlation between the potent anticancer activity of these compounds and their ability to inhibit the STAT3 pathway. Similar effects were observed in SB-590885-sensitive and SB-590885-resistant MEL 1617 cell lines (Figure 7A).

The inability of **7g**, **7h**, and **7i** to inhibit STAT3 phosphorylation in-cells suggests that their anticancer activities are predominantly due to their ability to release NO. Noticeably, when **7g** loses its ability to donate NO (compare to the corresponding ketone **6g**), it shows no anticancer activity (**6g** exhibited average growth inhibition of 2% in Table S1). The potent activity of **7b** and **7c** can, therefore, be attributed to a combination of STAT3 pathway inhibition and NO

production. As expected, **7b** and **7c** showed a similar ability to inhibit the phosphorylation of STAT3 in both SB-590885-sensitive and SB-590885-resistant cell lines, with more potent inhibitory activity towards the phosphorylation of Y705 than S727.

**Inhibition of STAT3-dependent luciferase reporter expression in both SB-590885-sensitive and resistant cell lines** - To further examine if **7b** and **7c** are potent STAT3 inhibitors in both SB-590885-sensitive and SB-590885-resistant cell lines, we evaluated their dose-response effect on the activity of a STAT3 promoter, using a dual-luciferase reporter assay. The STAT3 transcription activity in the four cell lines was estimated after the transient transfection of a mixture of an inducible STAT3-responsive firefly luciferase construct and a constitutively active renilla luciferase construct. As shown Figure 8A and in the table in Figure 7B, **7b** and **7c** inhibited STAT3 transcription in both 451-Lu-S and 451 Lu-R cell lines with similar potencies ( $IC_{50}$ 's are  $6.3 \pm 0.7 \mu\text{M}$  and  $4.7 \pm 0.8 \mu\text{M}$  for **7b** and  $7.9 \pm 1.3$  and  $17.0 \pm 3.0 \mu\text{M}$  for **7c**, respectively). A comparable effect of the two inhibitors was observed on the other two cell lines (MEL 1617-S and MEL 1617-R), **7b** exhibited  $IC_{50}$ 's of  $10.3 \pm 2.4$  and  $9.9 \pm 1.3 \mu\text{M}$ , and **7c** showed  $IC_{50}$ 's of  $21.4 \pm 4$  and  $15.6 \pm 4 \mu\text{M}$ , respectively. The control inhibitor **7g** showed a limited ability to inhibit STAT3 transcription in all the cell lines tested ( $IC_{50}$ 's in the range of 35–70  $\mu\text{M}$ ), suggesting that the sensitivity of the anticancer activity of these inhibitors resides in their ability to both inhibit STAT3 and release NO at the same time. However, we cannot rule out the possibility that the presence of the oxime structure itself is responsible for the enhanced anticancer activity of these STAT3 inhibitors.



**B. Inhibitory Activity on STAT3 Transcription and Melanoma Cells growth.**

Cell Line		Comp 7b	Comp 7c	Comp 7g	PLX-4720
451 Lu-S	*STAT3 Transcription IC <sub>50</sub> (μM)	6.3±0.66	7.9±1.3	54.0±19.0	N.A
	Growth Inhibition IC <sub>50</sub> (μM)	1.77±1.07	11.3±5.2	> 50	0.062±0.06
451 Lu-R	*STAT3 Transcription IC <sub>50</sub> (μM)	4.7±0.8	17.0±3.0	40.5±6.0	N.A
	Growth Inhibition IC <sub>50</sub> (μM)	7.8±3.5	47±8.4	>50	No Inhibition
MEL 1617-S	*STAT3 Transcription IC <sub>50</sub> (μM)	10.3±2.4	21.4±4	75±11	N.A
	Growth Inhibition IC <sub>50</sub> (μM)	8.4±3.5	46.1±10	>50	0.084±0.01
MEL 1617-R	*STAT3 Transcription IC <sub>50</sub> (μM)	9.9±1.3	15.6±4.0	35.2±5	N.A
	Growth Inhibition IC <sub>50</sub> (μM)	10.78±2.5	54.1±15	>50	No Inhibition

\*STAT3-dependent luciferase reporter gene assay in melanoma cell lines. N.A-Not Applicable.

**Figure 7:** (A) Compounds **7b**, **7c**, and **7g** inhibited STAT3 phosphorylation and PAX3 expression in melanoma cell lines with SB-590885 acquired resistance. Sensitive and resistant 451 Lu and MEL 1617 melanoma cell lines were exposed to different doses of each inhibitor for 12 hours before cell lysis. Protein expression of STAT3, phospho-STAT3, and PAX3 were analyzed by western blot using actin as a loading control. (Experiment was repeated at least two times) (B) This table represents the inhibitory activity of **7b**, **7c**, and **7g** towards the growth and

the STAT3 transcription activity of the Sensitive and resistant 451 Lu and MEL 1617 melanoma cell lines.

**The new hybrids inhibited proliferation of melanoma cell lines with acquired resistance to BRAF-inhibition** - We have demonstrated that **7b** and **7c** block STAT3 signal activation in four cell lines. Consistent with this, STAT3–PAX3 inhibition by **7b** and **7c** resulted in growth inhibition (Figure S1 and 7B) in both SB-590885-resistant and SB-590885-sensitive cell lines. The IC<sub>50</sub>'s of sensitive cell lines 451 Lu-S and MEL 1617-S were 1.8 and 8.4 μM for **7b**, 11.3, and 46.1 μM for **7c** and 0.06 and 0.084 μM for PLX-4720 respectively. The IC<sub>50</sub>'s of the resistant 451 Lu-R and MEL 1617-R cell lines that did not exhibit any growth inhibition by PLX-4720 were 7.8 and 10.8 μM for **7b** and 47 and 54 μM for **7c** respectively, which are similar to the IC<sub>50</sub>'s of inhibition of the sensitive cell lines by the same compounds. This suggests the capability of these inhibitors to overcome the acquired resistance to SB-590885. Noticeably, **7g** did not show any growth inhibition for any tested cell lines up to a concentration of 50 μM.

It has been reported that MEL1617-R cells exhibit more resistance to the MEK inhibitor GSK1120212 than MEL1617-S cells. In order to impede ERK phosphorylation and cell viability, and to induce G0/G1 cell cycle arrest, 10-fold more of GSK1120212 was required<sup>43</sup>. Interestingly, comparable cytotoxic effects of the STAT3 inhibitors, **7b** and **7c**, were observed in both cell lines (Figure S1 and 7B). The similar effect of the inhibitors on STAT3 phosphorylation and transcription activity in the two cell lines (Figures 7A, 7B, and 8A) is consistent with the notion that some BRAF inhibitor-resistant cells lines may exhibit less resistance to STAT3 inhibitors than to MEK inhibitors.

We also performed MTS assays to monitor the effect of the inhibitors on cell proliferation at different time points (Figure S2). Each cell line has been incubated with three concentrations of **7b** (DMSO, 1, 5, and 50 μM), and the MTS assay was performed after 24, 48,

and 72 hours of incubation. The results represented in (Figure S2) indicated that compound **7b** was capable of effectively suppressing 451 Lu-S and R, MEL 1617-S and R cell proliferation in a dose-dependent manner, with comparable effect on both SB-590885 sensitive and resistant cell lines.

**7b favorably inhibited resistant melanoma cell survival by apoptosis induction -** Suppressing STAT3 signaling in several cancer cells resulted in growth arrest and apoptosis. To investigate the ability of **7b** to induce apoptosis in SB-590885 sensitive and resistant cell lines, we determined its ability to enhance the formation of cleaved PARP and caspase-7 using western blotting. As shown in Figure 8B, **7b** increased the formation of cleaved PARP and caspase-7 levels in both 451 Lu-S and R cell lines in a dose-dependent manner, suggesting the ability of **7b** to induce apoptosis of these cell lines. Furthermore, we established these results using the Caspase 3/7 activity assay using the Caspase-Glo 3/7 assay Kit (Promega). As shown in Figure 8C, compound **7b** induced caspase activity and apoptosis in 451 Lu resistant cell lines in a dose-dependent manner.

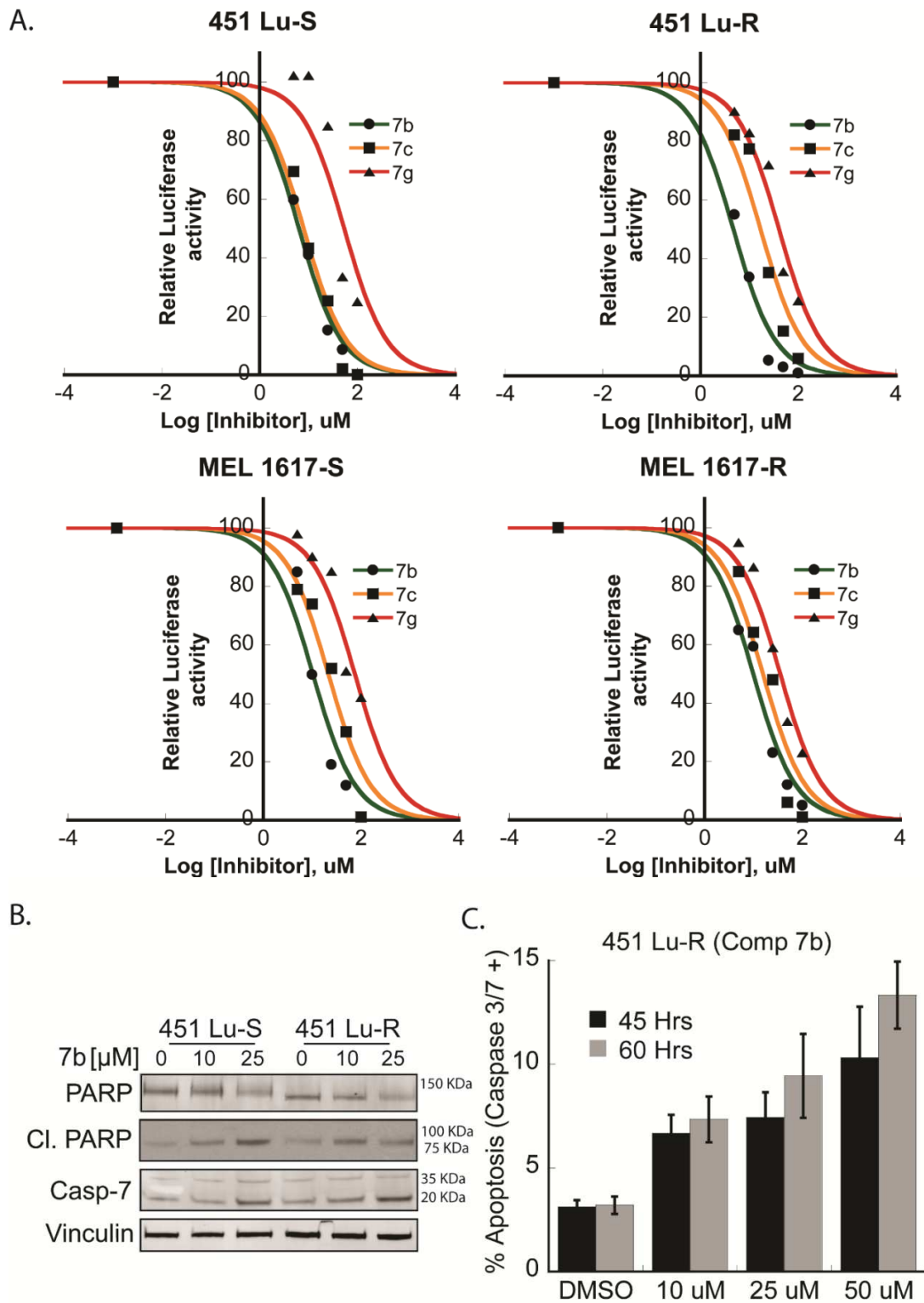


**Figure 8:** (A) Compounds **7b**, **7c**, and **7g** inhibited STAT3 signaling in melanoma cell lines with SB-590885-acquired resistance. Sensitive and resistant 451 Lu and MEL 1617 melanoma cell lines were transfected with a mixture of inducible STAT3-responsive firefly luciferase construct

and constitutively expressing renilla luciferase construct (40:1), after 48 hours of transfection, cells were treated with different doses of each inhibitor with vehicle (DMSO). A dual-luciferase assay was performed. The dose-response curves represent STAT3 transcriptional activity (Experiments were done in triplicates). **(B-C) 7b** induced caspase activity and apoptosis in the 451 Lu-R cell line. **(B) 7b** induced PARP and caspase-7 cleavage in both sensitive and resistant 451 Lu cell lines. Cells were exposed to different doses of each inhibitor for 12 hours before cell lysis. Protein expression of PARP, cleaved PARP and Caspase-7 were analyzed by western blot using vinculin as a loading control. (Experiment was repeated two times). **(C)** Cells were treated with different doses of compound **7b**, and then Apoptosis was analyzed using the IncuCyte Caspase-3/7 reagent and IncuCyte® ZOOM equipment with a  $\times 10$  objective at indicated time points. Error bars: SEM (n = 4). The number of apoptotic cells was normalized to the percentage area coverage (confluency) at the final time point to account for cell proliferation. Caspase-3/7 activity was significantly increased in a dose-dependent manner. Error bars: SEM (n = 3).

### 3. Conclusion

Here we report the synthesis of several hybrid compounds with an ability to simultaneously inhibit STAT3 signaling and to release NO into cells. **7b** and **7c** showed promising anticancer activity in several cell lines. Direct binding to STAT3 was confirmed using molecular docking studies, and a displacement assay using a FAM-labeled phosphopeptide that binds STAT3 in the SH2 domain. The new hybrids inhibited STAT3 tyrosine phosphorylation in several cancer cell lines. They did not affect the phosphorylation of other STAT isoforms. **7c** inhibited STAT3 nuclear translocation in mouse embryonic fibroblasts and STAT3 DNA binding in the A375 melanoma cell line. The sensitivity of cancer cells carrying a BRAF mutation to STAT3 inhibition was confirmed using these new inhibitors, **7b**, and **7c** which inhibited STAT3 phosphorylation in the A375 cell line carrying the V600E mutant after exposure to cytokine (IL-6), induced production of reactive oxygen species and arrested cell

growth at the G1 phase. These effects resulted in potent inhibition of A375 colonies formation by **7b** and **7c** in a dose-dependent manner. Moreover, **7b** and **7c** were able to inhibit cellular growth and proliferation and induce apoptosis of SB-590885-sensitive and resistant cell lines with comparable potency. This anticancer activity was attributed to their ability to both inhibit STAT3 transcription and release NO. The compounds discovered in this study may have potential as lead compounds for further development of dual-functional NO-releasing STAT3 inhibitors for treating BRAF-inhibitor resistant melanomas and/or other resistant types of cancer that is susceptible to STAT3 inhibition.

#### **4. Materials and Methods**

##### **4.1. Chemistry:**

Chemicals and solvents are of analytical grade. Melting points were determined on a Stuart electro-thermal melting point apparatus and were uncorrected. IR spectra were performed on Nicolet iS5 (ATR) FT-IR spectrometer at the faculty of pharmacy, Minia University.  $^1\text{H}$  spectra were recorded on Bruker Advance III 400 MHz, faculty of Benisweif University and Burker AG, Switzerland, 500 MHz, faculty of Pharmaceutical Sciences, Umm Al-Qura University, Mecca, Saudi Arabia using TMS as a reference standard and DMSO- $d_6$  as solvent. Chemical shifts ( $\delta$ ) are expressed in parts per million (ppm), and coupling constants ( $J$ ) are expressed in Hertz. The signals are designated as follows: s, singlet; d, doublet; t, triplet; m, multiplet.  $^{13}\text{C}$  spectra were recorded on Burker AG, Switzerland, 125 MHz, Faculty of Pharmaceutical Sciences, Umm Al-Qura University, Mecca, Saudia Arabia using TMS as a reference standard, and DMSO- $d_6$  as the solvent. Chemical shifts ( $\delta$ ) are expressed in parts per million (ppm). Electron ionization mass

spectra were collected in the Faculty of Pharmaceutical Sciences, University of British Columbia, Vancouver, Canada.

### **General procedure for the synthesis of compounds 1a-f**

A mixture of isatin or 5-methoxyisatin (10 mmol), 33% potassium hydroxide (10 mL) in ethanol (20 mL), and appropriate acetophenone derivative (10 mmol) was heated under reflux for 9-18 h. The reaction mixture was concentrated under reduced pressure, and the residue was diluted with water (50 mL) and extracted with ether (3 x 50 mL). The aqueous layer was neutralized with 1 M hydrochloric acid. The formed precipitate was filtered off, washed with water, dried, and crystallized from ethanol.

#### **2-Phenylquinoline-4-carboxylic acid (1a)**<sup>44</sup>.

White needles (0.19 g; 80 % yield); m.p. 212-214 °C; reported 208-210 °C.

#### **2-(4-Chlorophenyl)quinoline-4-carboxylic acid (1b)**<sup>44</sup>.

Pale yellow powder (0.24 g; 85 % yield); m.p. 144-146 °C; reported 142-144 °C.

#### **2-(4-Methoxyphenyl)quinoline-4-carboxylic acid (1c)**<sup>44</sup>.

White powder (0.22 g; 72 % yield); m.p. 197-198 °C; reported 195-196 °C.

#### **2-(4-Chlorophenyl)-6-methoxyquinoline-4-carboxylic acid (1d)**<sup>45</sup>.

White powder (0.22 g; 71 % yield); m.p. 265-267 °C; reported 264-266 °C.

#### **6-Methoxy-2-(4-methoxyphenyl)quinoline-4-carboxylic acid (1e)**<sup>45</sup>.

White powder (0.23 g; 75 % yield); m.p. 242-244 °C; reported 243-244 °C.

#### **2-(3,4-Dimethoxyphenyl)-6-methoxyquinoline-4-carboxylic acid (1f)**<sup>46</sup>.

Yellowish white powder (0.23 g; 70 % yield); m.p. 230-233 °C; reported 235 °C.

**General procedure for the synthesis of compounds (2a-f)**

A mixture of the appropriate 4-carboxylic acid **1a-f** (10 mmol), absolute ethanol (20 mL), and concentrated sulfuric acid (2 mL) was refluxed for 10 h. The solution was concentrated under reduced pressure; the mixture was allowed to cool at room temperature, diluted with water then rendered alkaline with a sodium bicarbonate solution. The formed precipitate was filtered off, washed with water and crystallized from ethanol.

**Ethyl 2-phenylquinoline-4-carboxylate (2a)**<sup>47</sup>.

Yellow liquid (0.20g; 75 % yield); m.p.; reported 51 °C.

**Ethyl 2-(4-chlorophenyl)quinoline-4-carboxylate (2b)**<sup>48</sup>.

White solid (0.24 g; 80 % yield); m.p. 79-81 °C; reported 72-73 °C.

**Ethyl 2-(4-methoxyphenyl)quinoline-4-carboxylate (2c)**<sup>49</sup>.

White solid (0.21 g; 69 % yield); m.p. 87-88 °C; reported 86-87 °C.

**Ethyl 2-(4-chlorophenyl)-6-methoxyquinoline-4-carboxylate (2d)**<sup>45</sup>.

White solid (0.28 g; 85 % yield); m.p. 129-130 °C; reported 128-129 °C.

**Ethyl 6-methoxy-2-(4-methoxyphenyl)quinoline-4-carboxylate (2e)**<sup>45</sup>.

Yellowish white solid (0.26 g; 79 % yield); m.p. 99-101 °C; reported 96-98 °C.

**Ethyl 2-(3,4-dimethoxyphenyl)-6-methoxyquinoline-4-carboxylate (2f)**<sup>50</sup>.

Yellow solid (0.21 g; 59 % yield); m.p. 106-108 °C; reported 105-106 °C.

**General procedure for the synthesis of compounds (3a-f).**

To a solution of **2a-f** (10 mmol) in ethanol (20 mL), hydrazine monohydrate (97%, 3 mL) was added and refluxed for 3-7 h. After cooling, the formed precipitate was filtered off, washed with water dried, and crystallized from ethanol.

**2-Phenylquinoline-4-carbohydrazide (3a)**<sup>51</sup>.

White solid (0.22 g; 84 % yield); m.p. 225-226 °C; reported 222 °C.

**2-(4-Chlorophenyl)quinoline-4-carbohydrazide (3b)**<sup>52</sup>.

White solid (0.27 g; 91 % yield); m.p. 234-236 °C; reported 235-237 °C.

**2-(4-Methoxyphenyl)quinoline-4-carbohydrazide (3c)**<sup>52</sup>.

White solid (0.25 g; 87 % yield); m.p. 208-210 °C.

**2-(4-Chlorophenyl)-6-methoxyquinoline-4-carbohydrazide (3d)**<sup>45</sup>.

White solid (0.22 g; 78 % yield); m.p. 233-235 °C; reported 233-234 °C.

**6-Methoxy-2-(4-methoxyphenyl)quinoline-4-carbohydrazide (3e)**<sup>45</sup>.

White solid (0.21 g; 66 % yield); m.p. 158-160 °C; reported 159-161 °C.

**2-(3,4-Dimethoxyphenyl)-6-methoxyquinoline-4-carbohydrazide (3f)**

White solid (0.19 g; 55 % yield); m.p. 223-226 °C ; IR (KBr, cm<sup>-1</sup>): 3360, 3257 (NH, NH<sub>2</sub>), 1645 (CO); <sup>1</sup>H NMR (400 MHz, CDCl<sub>3</sub>) δ (ppm): 10.04 (s, 1H, CO-NH), 8.06 (s, 1H, Ar-H), 8.02 (d, *J* = 9.2 Hz 1H, Ar-H), 7.87 (s, 1H, Ar-H), 7.83 (d, *J* = 8.4 Hz, 1H, Ar-H), 7.65 (s, 1H, Ar-H),

7.46 (d,  $J = 9.2$  Hz, 1H, Ar-H), 7.11 (d,  $J = 8.4$  Hz 1H, Ar-H), 4.74 (s, 2H, NH<sub>2</sub>), 3.91 (s, 3H, -OCH<sub>3</sub>), 3.89 (s, 3H, -OCH<sub>3</sub>), 3.85 (s, 3H, -OCH<sub>3</sub>).

#### **General procedure for the synthesis of compounds (4a-i).**

The detailed synthesis and spectral analysis of these intermediates have been previously reported<sup>53</sup>. In brief, equimolar quantities of the appropriate carbohydrazide **3a-f** (100 mmol) and allyl or phenyl isothiocyanate (100 mmol) in 125 mL of absolute ethanol were heated under reflux for 4 h. The solvent was evaporated under vacuum. Then 100 mL of 2N NaOH solution was added. The solution was refluxed for 3 h. The reaction mixture was cooled and acidified to pH 2 with concentrated HCl. The formed precipitate was filtered off, washed with water, and recrystallized from ethanol.

#### **4-Phenyl-5-(2-phenylquinolin-4-yl)-4H-1,2,4-triazole-3-thiol (4a)<sup>54</sup>.**

Orange needles (0.22 g; 60 % yield); m.p. 280-281 °C; reported 278-280 °C.

#### **4-Allyl-5-(2-phenylquinolin-4-yl)-4H-1,2,4-triazole-3-thiol (4b)<sup>53</sup>.**

White solid (0.21 g; 62 % yield); m.p. 266-268 °C; reported 266-268 °C.

#### **4-Allyl-5-(2-(4-chlorophenyl)quinolin-4-yl)-4H-1,2,4-triazole-3-thiol (4c)<sup>53</sup>.**

Yellow solid (0.28 g; 75 % yield); m.p. 182-183 °C; reported 182-183 °C.

#### **5-(2-(4-Chlorophenyl)quinolin-4-yl)-4-phenyl-4H-1,2,4-triazole-3-thiol (4d)<sup>53</sup>.**

White solid (0.29 g; 70 % yield); m.p. 198-200 °C; reported 198-200 °C.

#### **5-(2-(4-Methoxyphenyl)quinolin-4-yl)-4-phenyl-4H-1,2,4-triazole-3-thiol (4e)<sup>53</sup>.**

White solid (0.28 g; 69 % yield); m.p. 260-266 °C; reported 260-266 °C.

**4.1.5.6 4-Allyl-5-(2-(4-methoxyphenyl)quinolin-4-yl)-4*H*-1,2,4-triazole-3-thiol (4f)<sup>53</sup>.**

White solid (0.23 g; 62 % yield); m.p. 135-136 °C; reported 135-136 °C.

**5-(2-(4-Chlorophenyl)-6-methoxyquinolin-4-yl)-4-phenyl-4*H*-1,2,4-triazole-3-thiol (4g)<sup>53</sup>.**

White solid (0.35 g; 79 % yield); m.p. 238-240 °C; reported 238-240 °C.

**5-(6-Methoxy-2-(4-methoxyphenyl)quinolin-4-yl)-4-phenyl-4*H*-1,2,4-triazole-3-thiol (4h)<sup>53</sup>.**

Yellow solid (0.31 g; 71 % yield); m.p. 269-271 °C; reported 269-271 °C.

**5-(2-(3,4-Dimethoxyphenyl)-6-methoxyquinolin-4-yl)-4-phenyl-4*H*-1,2,4-triazole-3-thiol (4i)<sup>53</sup>.**

Yellowish white solid (0.31 g; 66 % yield); m.p. 230-231 °C; reported 230-231 °C.

**Synthesis of *N*-(4-acetylphenyl)-2-bromoacetamide **5**<sup>55</sup>.**

To a stirred mixture of *p*-aminoacetophenone (0.85 g, 6.3 mmol) in dichloromethane (20 mL) and potassium carbonate (0.17 g, 1.3 mmol) in 100 mL water cooled in an ice bath, bromoacetyl bromide (1.86 g, 9.2 mmol) in 30 mL dichloromethane was added in a drop-wise manner with stirring over 30 minutes. Stirring was continued for 2 h at 0 °C, then at room temperature overnight. The reaction mixture was extracted with dichloromethane (3 x 50 mL), and the organic layer was washed with distilled water (2 x 50 mL), dried over anhydrous sodium sulfate, filtered off, evaporated on a rotary evaporator and the residue was recrystallized from 95 % ethanol to give compound **5**; off-white crystals (0.24 g, 95 % yield); m.p. 155 °C; reported 157 °C.

**General procedure for the synthesis of compounds (6a-i).**

An equimolar mixture of **4a-i**, compound **5** (1 mmol), and TEA (0.12 g, 1.2 mmol) in acetonitrile (50 mL) was heated at reflux for 4-8 h. The reaction mixture was evaporated to dryness. The residue was crystallized from aqueous ethanol affording compounds **6a-i**.

***N*-(4-Acetylphenyl)-2-((4-phenyl-5-(2-phenylquinolin-4-yl)-4*H*-1,2,4-triazol-3-yl)thio)acetamide (6a).**

White solid (0.36 g; 65 % yield); m.p. 124-126 °C; IR (KBr, cm<sup>-1</sup>): 3310 (NH), 1670 (COCH<sub>3</sub>), 1660 (CONH); <sup>1</sup>H NMR (500 MHz, DMSO-d<sub>6</sub>) δ (ppm): 10.79 (s, 1H, NH), 8.13-8.09 (m, 2H, Ar-H), 8.06 (s, 1H, Ar-H), 8.03 (d, *J* = 7.3 Hz, 2H, Ar-H), 7.97 (d, *J* = 8.6 Hz, 2H, Ar-H), 7.82 (t, *J* = 7.6 Hz, 1H, Ar-H), 7.76 (d, *J* = 8.6 Hz, 2H, Ar-H), 7.62 (t, *J* = 7.6 Hz, 1H, Ar-H), 7.50-7.48 (m, 5H, Ar-H), 7.48-7.41 (m, 3H, Ar-H), 4.37 (s, 2H, S-CH<sub>2</sub>), 2.54 (s, 3H, CO-CH<sub>3</sub>); <sup>13</sup>C NMR (125 MHz, DMSO-d<sub>6</sub>) δ (ppm): 197.01, 166.61, 155.68, 152.56, 152.32, 148.29, 143.57, 138.24, 133.66, 133.59, 132.47, 131.02, 130.55, 130.49, 130.43, 130.28, 130.07, 129.42, 127.99, 127.81, 127.47, 126.02, 124.99, 120.89, 118.90, 37.45, 26.93; Anal. Calcd. For C<sub>33</sub>H<sub>25</sub>N<sub>5</sub>O<sub>2</sub>S (555.65): C, 71.33; H, 4.53; N, 12.60; Found: C, 71.56; H, 4.61; N, 12.87; EI-MS (ESI) m/z: calcd. (555.66); Found: (555.20) (M<sup>+</sup>).

***N*-(4-Acetylphenyl)-2-((4-allyl-5-(2-phenylquinolin-4-yl)-4*H*-1,2,4-triazol-3-yl)thio)acetamide (6b).**

White solid (0.31 g; 60 % yield); m.p. 212-214 °C; IR (KBr, cm<sup>-1</sup>): 3311 (NH), 1681 (COCH<sub>3</sub>), 1658 (CONH); <sup>1</sup>H NMR (400 MHz, DMSO-d<sub>6</sub>) δ (ppm): 10.76 (s, 1H, NH), 8.32-8.29 (m, 3H, Ar-H), 8.20 (d, *J* = 8.4 Hz, 1H, Ar-H), 7.97 (d, *J* = 8.4 Hz, 2H, Ar-H), 7.89-7.84 (m, 2H, Ar-H), 7.76 (d, *J* = 8.4 Hz, 2H, Ar-H), 7.63-7.53 (m, 4H, Ar-H), 5.90-5.81 (m, 1H, CH<sub>2</sub>-CH=CH<sub>2</sub>), 5.11 (d, *J*<sub>cis</sub> = 10.4 Hz, 1H, CH=CH<sub>2</sub>), 4.83 (d, *J*<sub>trans</sub> = 17.2 Hz, 1H, CH=CH<sub>2</sub>), 4.66-4.63 (m, 2H, CH<sub>2</sub>-CH), 4.33 (s, 2H, S-CH<sub>2</sub>), 2.50 (s, 3H, CO-CH<sub>3</sub>); <sup>13</sup>C NMR (125 MHz, DMSO-d<sub>6</sub>) δ (ppm):

197.14, 168.06, 162.94, 156.93, 153.97, 153.28, 143.26, 138.84, 138.06, 134.17, 131.62, 130.45, 130.18, 130.03, 129.26, 129.02, 128.10, 128.04, 125.26, 120.64, 119.58, 119.16, 118.02, 47.98, 32.93, 27.78; Anal. Calcd. For C<sub>30</sub>H<sub>25</sub>N<sub>5</sub>O<sub>2</sub>S (519.62): C, 69.34, H, 4.85; N, 13.48; Found: C, 69.18; H, 4.92; N, 13.72.

***N*-(4-Acetylphenyl)-2-((4-allyl-5-(2-(4-chlorophenyl)quinolin-4-yl)-4*H*-1,2,4-triazol-3-yl)thio)acetamide (6c).**

White solid (0.49 g; 89 % yield); m.p. 191-192 °C; IR (KBr, cm<sup>-1</sup>): 3310 (NH), 1667 (COCH<sub>3</sub>), 1599 (CONH); <sup>1</sup>H NMR (500 MHz, DMSO-d<sub>6</sub>) δ (ppm): 10.79 (s, 1H, NH), 8.33 (d, *J* = 8.5 Hz, 2H, Ar-H), 8.31 (s, 1H, Ar-H), 8.20 (d, *J* = 8.2 Hz, 1H, Ar-H), 7.97 (d, *J* = 8.5 Hz, 2H, Ar-H), 7.88 (t, *J* = 7.7 Hz, 1H, Ar-H), 7.84 (d, *J* = 8.2 Hz, 1H, Ar-H), 7.76 (d, *J* = 8.5 Hz, 2H, Ar-H), 7.64 (d, *J* = 8.5 Hz, 2H, Ar-H), 7.63-7.61 (m, 1H, Ar-H), 5.86-5.79 (m, 1H, CH<sub>2</sub>-CH=CH<sub>2</sub>), 5.10 (d, *J*<sub>cis</sub> = 10.5 Hz, 1H, CH=CH<sub>2</sub>), 4.82 (d, *J*<sub>trans</sub> = 17.0 Hz, 1H, CH=CH<sub>2</sub>), 4.64-4.63 (m, 2H, CH<sub>2</sub>-CH), 4.33 (s, 2H, S-CH<sub>2</sub>), 2.54 (s, 3H, CO-CH<sub>3</sub>); <sup>13</sup>C NMR (125 MHz, DMSO-d<sub>6</sub>) δ (ppm): 197.01, 166.78, 154.90, 152.41, 151.62, 148.41, 143.56, 137.19, 135.48, 134.32, 132.61, 132.49, 131.24, 130.18, 130.06, 129.55, 129.48, 128.31, 125.67, 125.40, 120.08, 118.92, 118.01, 47.18, 38.25, 26.92; Anal. Calcd. For C<sub>30</sub>H<sub>24</sub>ClN<sub>5</sub>O<sub>2</sub>S (554.06): C, 65.03; H, 4.37; N, 12.64; Found: C, 65.28; H, 4.45; N, 12.89; EI-MS (ESI) *m/z*: calcd. (554.07); Found: (554.1) (M<sup>+</sup>).

***N*-(4-Acetylphenyl)-2-((5-(2-(4-chlorophenyl)quinolin-4-yl)-4-phenyl-4*H*-1,2,4-triazol-3-yl)thio)acetamide (6d).**

White solid (0.52 g; 89 % yield); m.p. 295-297 °C; <sup>1</sup>H NMR (500 MHz, DMSO-d<sub>6</sub>) δ (ppm): 10.80 (s, 1H, NH), 8.11-8.07 (m, 5H, Ar-H), 7.98 (d, *J* = 8.5 Hz, 2H, Ar-H), 7.83-7.81 (m, 1H, Ar-H), 7.77 (d, *J* = 8.7 Hz, 2H, Ar-H), 7.64-7.62 (m, 3H, Ar-H), 7.59 (d, *J* = 8.7 Hz, 2H, Ar-H), 7.54-7.42 (m, 3H, Ar-H), 4.38 (s, 2H, S-CH<sub>2</sub>), 2.55 (s, 3H, CO-CH<sub>3</sub>); <sup>13</sup>C NMR (125 MHz,

DMSO-d<sub>6</sub>)  $\delta$  (ppm): 197.01, 166.61, 154.45, 152.59, 152.27, 148.20, 143.58, 137.03, 135.46, 133.92, 133.53, 132.47, 131.16, 130.56, 130.26, 130.08, 130.01, 129.49, 129.21, 128.21, 127.77, 126.01, 125.07, 120.81, 118.90, 37.43, 26.93; Anal. Calcd. For C<sub>33</sub>H<sub>24</sub>ClN<sub>5</sub>O<sub>2</sub>S (590.09) : C, 67.17; H, 4.10; N, 11.87; Found: C, 67.42; H, 4.17; N, 12.04; EI-MS (ESI) m/z: calcd. (590.09); Found: (590.10) (M<sup>+</sup>).

***N*-(4-Acetylphenyl)-2-((5-(2-(4-methoxyphenyl)quinolin-4-yl)-4-phenyl-4*H*-1,2,4-triazol-3-yl)thio)acetamide (6e).**

White solid (0.50 g; 87 % yield); m.p. 185-187 °C; <sup>1</sup>H NMR (500 MHz, DMSO-d<sub>6</sub>)  $\delta$  (ppm): 10.81 (s, 1H, NH), 8.08-8.06 (m, 3H, Ar-H), 8.04-7.96 (m, 4H, Ar-H), 7.82-7.76 (m, 3H, Ar-H), 7.57 (t, *J* = 7.3 Hz, 1H, Ar-H), 7.52-7.49 (m, 5H, Ar-H), 7.07 (d, *J* = 8.0 Hz, 2H, Ar-H), 4.37 (s, 2H, S-CH<sub>2</sub>), 3.84 (s, 3H, O-CH<sub>3</sub>), 2.55 (s, 3H, CO-CH<sub>3</sub>); <sup>13</sup>C NMR (125 MHz, DMSO-d<sub>6</sub>)  $\delta$  (ppm): 197.01, 166.62, 161.42, 155.37, 152.47, 152.42, 148.30, 143.58, 133.61, 133.49, 132.50, 130.87, 130.69, 130.53, 130.25, 130.05, 129.78, 128.96, 127.80, 127.49, 125.94, 124.68, 120.50, 118.93, 114.82, 55.83, 37.49, 26.91; Anal. Calcd. For C<sub>34</sub>H<sub>27</sub>N<sub>5</sub>O<sub>3</sub>S (585.68): C, 69.73; H, 4.65; N, 11.96; Found: C, 69.98; H, 4.67; N, 12.28; EI-MS (ESI) m/z: calcd. (585.68); Found: (585.5) (M<sup>+</sup>).

***N*-(4-Acetylphenyl)-2-((4-allyl-5-(2-(4-methoxyphenyl)-quinolin-4-yl)-4*H*-1,2,4-triazol-3-yl)thio)acetamide (6f).**

White solid (0.45 g; 83 % yield); m.p. 214-216 °C; <sup>1</sup>H NMR (500 MHz, DMSO-d<sub>6</sub>)  $\delta$  (ppm): 10.79 (s, 1H, NH), 8.27 (d, *J* = 8.8 Hz, 2H, Ar-H), 8.23 (s, 1H, Ar-H), 8.14 (d, *J* = 8.4 Hz, 1H, Ar-H), 7.97 (d, *J* = 8.6 Hz, 2H, Ar-H), 7.84 (t, *J* = 7.6 Hz, 1H, Ar-H), 7.80 (d, *J* = 8.4 Hz, 1H, Ar-H), 7.76 (d, *J* = 8.6 Hz, 2H, Ar-H), 7.57 (t, *J* = 7.6 Hz, 1H, Ar-H), 7.12 (d, *J* = 8.8 Hz, 2H, Ar-H), 5.88-5.81 (m, 1H, CH<sub>2</sub>-CH=CH<sub>2</sub>), 5.11 (d, *J*<sub>cis</sub> = 10.5 Hz, 1H, -CH=CH<sub>2</sub>), 4.83 (d, *J*<sub>trans</sub> =

17.2 Hz, 1H, -CH=CH<sub>2</sub>), 4.62-4.60 (m, 2H, CH<sub>2</sub>-CH), 4.33 (s, 2H, S-CH<sub>2</sub>), 3.86 (s, 3H, O-CH<sub>3</sub>), 2.54 (s, 3H, CO-CH<sub>3</sub>); <sup>13</sup>C NMR (125 MHz, DMSO-d<sub>6</sub>) δ (ppm): 197.01, 166.80, 161.47, 155.75, 152.59, 151.52, 148.49, 143.56, 133.92, 132.64, 132.49, 130.98, 130.80, 130.06, 129.95, 129.26, 127.60, 125.59, 124.96, 119.73, 118.92, 117.98, 114.84, 55.84, 47.18, 38.29, 26.92; Anal. Calcd. For C<sub>31</sub>H<sub>27</sub>N<sub>5</sub>O<sub>3</sub>S (549.64): C, 67.74; H, 4.95; N, 12.74; Found: C, 68.01; H, 4.88; N, 12.98.

***N*-(4-Acetylphenyl)-2-((5-(2-(4-chlorophenyl)-6-methoxy-quinolin-4-yl)-4-phenyl-4*H*-1,2,4-triazol-3-yl)thio)acetamide (6g).**

Yellowish white solid (0.55 g; 90 % yield); m.p. 224-225 °C; <sup>1</sup>H NMR (500 MHz, DMSO-d<sub>6</sub>) δ (ppm): 9.57 (s, 1H, NH), 7.95 (s, 1H, ArH), 7.93-7.91 (m, 4H, Ar-H), 7.84 (d, *J* = 7.5 Hz, 1H, Ar-H), 7.61 (d, *J* = 7.5 Hz, 2H, Ar-H), 7.60-7.58 (m, 1H, Ar-H), 7.54-7.51 (m, 2H, Ar-H), 7.45 (d, *J* = 7.5 Hz, 2H, Ar-H), 7.35 (s, 1H, Ar-H), 7.16 (t, *J* = 7.5 Hz, 2H, Ar-H), 7.05 (t, *J* = 7.4 Hz, 1H, Ar-H), 3.99 (s, 2H, CH<sub>2</sub>-S), 3.81 (s, 3H, O-CH<sub>3</sub>), 2.49 (s, 3H, CO-CH<sub>3</sub>); <sup>13</sup>C NMR (125 MHz, DMSO-d<sub>6</sub>) δ (ppm) 197.00, 166.65, 162.95, 158.68, 151.92, 144.40, 143.55, 137.19, 134.92, 133.69, 133.29, 131.69, 130.49, 130.27, 130.04, 130.01, 129.39, 128.84, 127.67, 126.26, 123.53, 121.08, 119.64, 118.93, 103.90, 56.20, 37.54, 26.91; Anal. Calcd. For C<sub>34</sub>H<sub>26</sub>ClN<sub>5</sub>O<sub>3</sub>S (620.12): C, 65.85; H, 4.23; N, 11.29; Found: C, 66.08; H, 4.31; N, 11.57.

***N*-(4-Acetylphenyl)-2-((5-(6-methoxy-2-(4-methoxyphenyl)-quinolin-4-yl)-4-phenyl-4*H*-1,2,4-triazol-3-yl)thio)acetamide (6h).**

Yellowish white solid (0.44 g; 73 % yield); m.p. 229-230 °C; <sup>1</sup>H NMR (500 MHz, DMSO-d<sub>6</sub>) δ (ppm): 10.79 (s, 1H, NH), 7.95-7.93 (m, 6H, Ar-H), 7.75 (d, *J* = 7.9 Hz, 2H, Ar-H), 7.50-7.38 (m, 9H, Ar-H), 7.04 (d, *J* = 7.9 Hz, 2H, Ar-H), 4.36 (s, 2H, S-CH<sub>2</sub>), 3.85 (s, 3H, OCH<sub>3</sub>), 3.82 (s, 3H, OCH<sub>3</sub>), 2.54 (s, 3H, CO-CH<sub>3</sub>); <sup>13</sup>C NMR (125 MHz, DMSO-d<sub>6</sub>) δ (ppm): 197.14, 168.06,

164.02, 162.50, 159.48, 159.17, 156.10, 152.74, 143.26, 137.40, 137.19, 131.62, 131.14, 130.69, 130.59, 130.18, 130.07, 128.75, 128.40, 128.01, 121.29, 120.88, 119.58, 114.11, 104.91, 56.04, 32.93, 27.79; Anal. Calcd. For C<sub>35</sub>H<sub>29</sub>N<sub>5</sub>O<sub>4</sub>S (615.70): C, 68.28; H, 4.75; N, 11.37; Found: C, 68.54; H, 4.87; N, 11.49; EI-MS (ESI) m/z: calcd. (615.71); Found: (615.1) (M<sup>+</sup>).

***N*-(4-Acetylphenyl)-2-((5-(2-(3,4-dimethoxyphenyl)-6-methoxyquinolin-4-yl)-4-phenyl-4*H*-1,2,4-triazol-3-yl)thio)acetamide (6i).**

Yellow solid (0.39 g; 62 % yield); m.p. 150-151 °C; <sup>1</sup>H NMR (500 MHz, DMSO-d<sub>6</sub>) δ (ppm): 10.79 (s, 1H, NH), 8.00-7.97 (m, 4H, Ar-H), 7.76 (d, *J* = 8.3 Hz, 2H, Ar-H), 7.60 (s, 1H, Ar-H), 7.56-7.52 (m, 3H, Ar-H), 7.44-7.41 (m, 5H, Ar-H), 7.06 (d, *J* = 8.3 Hz, 1H, Ar-H), 4.37 (s, 2H, S-CH<sub>2</sub>), 3.86 (s, 6H, OCH<sub>3</sub>), 3.82 (s, 3H, OCH<sub>3</sub>), 2.55 (s, 3H, CO-CH<sub>3</sub>); <sup>13</sup>C NMR (125 MHz, DMSO-d<sub>6</sub>) δ (ppm): 197.01, 166.66, 158.20, 152.99, 152.73, 152.39, 150.77, 149.48, 144.39, 143.55, 133.75, 132.51, 132.00, 131.46, 131.02, 130.49, 130.26, 130.04, 127.70, 125.77, 123.09, 120.91, 120.03, 118.93, 112.27, 110.25, 104.04, 56.12, 56.08, 37.49, 26.91; Anal. Calcd. For C<sub>36</sub>H<sub>31</sub>N<sub>5</sub>O<sub>5</sub>S (645.73): C, 66.96; H, 4.84; N, 10.85; Found: C, 67.21; H, 4.92; N, 11.07.

**General procedure for the synthesis of compounds (7a-i)**<sup>56</sup>.

A mixture of equimolar amounts of the appropriate ketone **6a-i** (1.00 mmol), hydroxylamine hydrochloride (0.35 g, 5.00 mmol) and anhydrous sodium acetate (0.08 g, 1.00 mmol) in absolute ethanol (30 mL) was heated under reflux for 8-12 h then left to cool. The separated solid was filtered off, washed with dil. ammonia solution (10 %), dried and crystallized from aqueous ethanol affording the pure novel products **7a-i**.

***N*-(4-(1-(Hydroxyimino)ethyl)phenyl)-2-((4-phenyl-5-(2-phenylquinolin-4-yl)-4*H*-1,2,4-triazol-3-yl)thio)acetamide (7a).**

White solid (0.33 g; 59 % yield); m.p. 158-160 °C; IR (KBr, cm<sup>-1</sup>): 3243 (OH, NH), 1660 (CONH); <sup>1</sup>H NMR (500 MHz, DMSO-*d*<sub>6</sub>) δ (ppm): 11.11 (s, 1H, OH), 10.57 (s, 1H, NH), 8.13 (d, *J* = 8.4 Hz, 2H, Ar-H), 8.10 (d, *J* = 8.4 Hz, 2H, Ar-H), 8.06 (s, 1H, Ar-H), 7.03 (d, *J* = 7.1 Hz, 1H, Ar-H), 7.82 (t, *J* = 7.1 Hz, 1H, Ar-H), 7.64-7.60 (m, 4H, Ar-H), 7.51-7.49 (m, 5H, Ar-H), 7.45-7.42 (m, 3H, Ar-H), 4.35 (s, 2H, S-CH<sub>2</sub>), 2.14 (s, 3H, -CH<sub>3</sub>); <sup>13</sup>C NMR (125 MHz, DMSO-*d*<sub>6</sub>) δ (ppm): 166.04, 155.68, 152.87, 152.64, 152.30, 148.30, 139.64, 138.24, 133.68, 133.61, 132.59, 131.01, 130.53, 130.49, 130.27, 130.01, 129.42, 127.99, 127.82, 127.48, 126.60, 126.03, 125.01, 120.89, 119.30, 37.46, 11.85; Anal. Calcd. For C<sub>33</sub>H<sub>26</sub>N<sub>6</sub>O<sub>2</sub>S (570.66): C, 69.45, H, 4.59; N, 14.73; Found: C, 69.72; H, 4.55; N, 15.01.

**2-((4-Allyl-5-(2-phenylquinolin-4-yl)-4*H*-1,2,4-triazol-3-yl)-thio)-*N*-(4-(1-(hydroxyimino)ethyl)phenyl)acetamide (7b).**

Yellowish white solid (0.29 g; 55 % yield); m.p. 175-178 °C; IR (KBr, cm<sup>-1</sup>): 3249 (OH, NH), 1658 (CONH); <sup>1</sup>H NMR (600 MHz, DMSO-*d*<sub>6</sub>) δ (ppm): 11.11 (s, 1H, NH), 10.53 (s, 1H, OH), 8.31 (d, *J* = 7.2 Hz, 2H, Ar-H), 8.29 (s, 1H, Ar-H), 8.21 (d, *J* = 8.4 Hz, 1H, Ar-H), 7.88 (t, *J* = 7.5 Hz, 1H, Ar-H), 7.85 (d, *J* = 8.4 Hz, 1H, Ar-H), 7.68-7.61 (m, 5H, Ar-H), 7.60-7.53 (m, 3H, Ar-H), 5.88-5.82 (m, 1H, CH<sub>2</sub>-CH=CH<sub>2</sub>), 5.12 (d, *J*<sub>cis</sub> = 10.2 Hz, 1H, CH=CH<sub>2</sub>), 4.83 (d, *J*<sub>trans</sub> = 17.4 Hz, 1H, CH=CH<sub>2</sub>), 4.64 (d, *J* = 3.6 Hz, 2H, CH<sub>2</sub>-CH), 4.30 (s, 2H, S-CH<sub>2</sub>), 2.14 (s, 3H, CH<sub>3</sub>); <sup>13</sup>C NMR (151 MHz, DMSO-*d*<sub>6</sub>) δ (ppm): 166.21, 156.10, 152.85, 152.49, 151.62, 148.49, 139.58, 138.39, 134.17, 132.67, 131.09, 130.52, 130.18, 129.53, 129.44, 128.08, 127.78, 126.59, 125.65, 125.32, 120.14, 119.34, 117.96, 47.19, 38.35, 11.85; Anal. Calcd. For C<sub>30</sub>H<sub>26</sub>N<sub>6</sub>O<sub>2</sub>S (534.63): C, 67.40; H, 4.90; N, 15.72; Found: C, 67.65; H, 4.98; N, 16.04.

**2-((4-Allyl-5-(2-(4-chlorophenyl)quinolin-4-yl)-4H-1,2,4-triazol-3-yl)thio)-N-(4-(1-(hydroxyimino)ethyl)phenyl)acetamide (7c).**

White solid (0.39 g; 70 % yield); m.p. 232-234 °C; IR (KBr,  $\text{cm}^{-1}$ ): 3371 (OH, NH), 1557 ( $\text{CONH}$ );  $^1\text{H}$  NMR (600 MHz,  $\text{DMSO-}d_6$ )  $\delta$  (ppm):  $^1\text{H}$  NMR (600 MHz,  $\text{DMSO-}d_6$ )  $\delta$  (ppm): 11.11 (s, 1H, NH), 10.53 (s, 1H, OH), 8.34 (d,  $J = 9.0$  Hz, 2H, Ar-H), 8.32 (s, 1H, Ar-H), 8.20 (d,  $J = 8.4$  Hz, 1H, Ar-H), 7.90–7.87 (m, 1H, Ar-H), 7.84 (d,  $J = 8.4$  Hz, 1H, Ar-H), 7.65–7.62 (m, 7H, Ar-H), 5.86–5.80 (m, 1H,  $\text{CH}_2\text{-CH=CH}_2$ ), 5.10 (d,  $J_{\text{cis}} = 10.2$  Hz, 1H,  $\text{CH=CH}_2$ ), 4.82 (d,  $J_{\text{trans}} = 16.8$  Hz, 1H,  $\text{CH=CH}_2$ ), 4.64 (d,  $J = 4.8$  Hz, 2H,  $\text{CH}_2\text{-CH}$ ), 4.30 (s, 2H, S- $\text{CH}_2$ ), 2.14 (s, 3H,  $\text{CH}_3$ );  $^{13}\text{C}$  NMR (151 MHz,  $\text{DMSO-}d_6$ )  $\delta$  (ppm): 166.19, 154.90, 152.84, 152.39, 151.65, 148.41, 139.59, 137.20, 135.48, 134.36, 132.63, 131.21, 130.18, 129.54, 129.46, 128.29, 126.59, 125.67, 125.41, 120.08, 119.33, 118.93, 118.01, 47.19, 38.33, 11.85; Anal. Calcd. For  $\text{C}_{30}\text{H}_{25}\text{ClN}_6\text{O}_2\text{S}$  (569.08): C, 63.32; H, 4.43; N, 14.77; Found: C, 63.59; H, 4.40; N, 14.89.

**2-((5-(2-(4-Chlorophenyl)quinolin-4-yl)-4-phenyl-4H-1,2,4-triazol-3-yl)thio)-N-(4-(1-(hydroxyimino)ethyl)phenyl)acetamide (7d).**

Off-white solid (0.48 g; 80 % yield); m.p. 178-179 °C;  $^1\text{H}$  NMR (500 MHz,  $\text{DMSO-}d_6$ )  $\delta$  (ppm): 11.10 (s, 1H, OH), 10.40 (s, 1H, NH), 8.08 (d,  $J = 7.5$  Hz, 1H, Ar-H), 8.02 -7.98 (m, 2H, Ar-H), 7.90-7.88 (m, 3H, Ar-H), 7.80 (d,  $J = 7.5$  Hz, 1H, Ar-H), 7.66 -7.62 (m, 2H, Ar-H), 7.59 -7.54 (m, 3H, Ar-H), 7.47-7.43 (m, 2H, Ar-H), 7.40 (t,  $J = 7.5$  Hz, 1H, Ar-H), 7.14-7.09 (m, 3H, Ar-H), 4.00 (s, 2H, S- $\text{CH}_2$ ), 2.27 (s, 3H,  $\text{-CH}_3$ );  $^{13}\text{C}$  NMR (125 MHz,  $\text{DMSO-}d_6$ )  $\delta$  (ppm): 168.06, 164.02, 163.36, 159.48, 156.33, 153.99, 138.82, 138.73, 137.40, 135.59, 135.10, 130.41, 130.07, 130.03, 129.69, 129.58, 129.26, 128.75, 128.40, 128.21, 126.44, 125.26, 121.23, 120.64, 119.61, 32.93, 17.67; Anal. Calcd. For  $\text{C}_{33}\text{H}_{25}\text{ClN}_6\text{O}_2\text{S}$  (605.11): C, 65.50; H, 4.16; N, 13.89; Found: C, 65.78; H, 4.11; N, 14.08.

***N*-(4-(1-(Hydroxyimino)ethyl)phenyl)-2-((5-(2-(4-methoxy-phenyl)quinolin-4-yl)-4-phenyl-4*H*-1,2,4-triazol-3-yl)thio)acetamide (7e).**

Yellow solid (0.45 g; 75 % yield); m.p. 175-178 °C; <sup>1</sup>H NMR (500 MHz, DMSO-*d*<sub>6</sub>) δ (ppm): 11.12 (s, 1H, OH), 10.59 (s, 1H, NH), 8.05 (d, *J* = 8.4 Hz, 2H, Ar-H), 8.01-7.99 (m, 3H, Ar-H), 7.78 (t, *J* = 7.6 Hz, 1H, Ar-H), 7.66-7.63 (m, 4H, Ar-H), 7.57 (t, *J* = 7.6 Hz, 1H, Ar-H), 7.49 (d, *J* = 5.4 Hz, 2H, Ar-H), 7.44-7.41 (m, 2H, Ar-H), 7.29-7.09 (m, 1H, Ar-H), 7.06 (d, *J* = 8.8 Hz, 2H, Ar-H), 4.32 (s, 2H, S-CH<sub>2</sub>), 3.83 (s, 3H, -OCH<sub>3</sub>), 2.13 (s, 3H, -CH<sub>3</sub>); <sup>13</sup>C NMR (125 MHz, DMSO-*d*<sub>6</sub>) δ (ppm): 166.08, 161.42, 155.36, 152.96, 152.56, 152.37, 148.17, 139.60, 133.56, 132.59, 130.97, 130.55, 130.24, 130.00, 129.67, 129.01, 128.20, 127.77, 127.56, 126.60, 125.92, 124.65, 120.53, 119.33, 114.83, 55.82, 37.43, 11.86; Anal. Calcd. For C<sub>34</sub>H<sub>28</sub>N<sub>6</sub>O<sub>3</sub>S (600.69): C, 67.98; H, 4.70; N, 13.99; Found: C, 68.27; H, 4.76; N, 14.32.

**2-((4-Allyl-5-(2-(4-methoxyphenyl)quinolin-4-yl)-4*H*-1,2,4-triazol-3-yl)thio)-*N*-(4-(1-(hydroxyimino)ethyl)phenyl)acetamide (7f).**

White solid (0.33 g; 59 % yield); m.p. 224-226 °C; <sup>1</sup>H NMR (500 MHz, DMSO-*d*<sub>6</sub>) δ (ppm): 11.10 (s, 1H, OH), 10.19 (s, 1H, NH), 8.12 (d, *J* = 7.5 Hz, 1H, Ar-H), 7.91 (d, *J* = 7.5 Hz, 2H, Ar-H), 7.86 (d, *J* = 7.5 Hz, 1H, Ar-H), 7.82 (d, *J* = 7.5 Hz, 2H, Ar-H), 7.64 (t, *J* = 7.5 Hz, 1H, Ar-H), 7.56 (s, 1H, Ar-H), 7.49 (t, *J* = 7.5 Hz, 1H, Ar-H), 7.44 (d, *J* = 7.5 Hz, 2H, Ar-H), 7.04 (d, *J* = 7.5 Hz, 2H, Ar-H), 5.84-5.76 (m, 1H, -CH<sub>2</sub>-CH=CH<sub>2</sub>), 5.11 (d, *J*<sub>trans</sub> = 14.0 Hz, 1H, -CH=CH<sub>2</sub>), 5.06 (d, *J*<sub>cis</sub> = 11.0 Hz, 1H, -CH=CH<sub>2</sub>), 4.55 (d, *J* = 5.2 Hz, 2H, CH<sub>2</sub>-CH=CH<sub>2</sub>), 4.01 (s, 2H, S-CH<sub>2</sub>), 3.78 (s, 3H, OCH<sub>3</sub>), 2.28 (s, 3H, CNCH<sub>3</sub>); <sup>13</sup>C NMR (125 MHz, DMSO-*d*<sub>6</sub>) δ (ppm): 168.06, 162.94, 162.50, 156.93, 156.33, 153.97, 153.29, 138.84, 138.82, 134.17, 131.14, 130.03, 129.26, 128.22, 128.04, 128.01, 126.45, 125.26, 120.64, 119.62, 119.17, 118.03, 114.10,

56.04, 47.98, 32.93, 17.67; Anal. Calcd. For  $C_{31}H_{28}N_6O_3S$  (564.66): C, 65.94; H, 5.00; N, 14.88; Found: C, 65.87; H, 4.94; N, 15.03.

**2-((5-(2-(4-Chlorophenyl)-6-methoxyquinolin-4-yl)-4-phenyl-4*H*-1,2,4-triazol-3-yl)thio)-*N*-(4-(1-(hydroxyimino)ethyl)phenyl) acetamide (7g).**

Yellow solid (0.50 g; 80 % yield); m.p. 267-268 °C;  $^1H$  NMR (500 MHz, DMSO- $d_6$ )  $\delta$  (ppm): 11.10 (s, 1H, OH), 10.56 (s, 1H, NH), 8.05-7.99 (m, 3H, Ar-H), 7.75 (d,  $J = 8.4$  Hz, 1H), 7.64-7.61 (m, 3H, Ar-H), 7.56 (d,  $J = 8.0$  Hz, 2H, Ar-H), 7.51 (d,  $J = 8.0$ , 2H, Ar-H), 7.45-7.41 (m, 5H, Ar-H), 7.39 (s, 1H, Ar-H), 4.34 (s, 2H, S- $\underline{CH_2}$ ), 3.86 (s, 3H, - $\underline{OCH_3}$ ), 2.12 (s, 3H, - $\underline{CH_3}$ );  $^{13}C$  NMR (125 MHz, DMSO- $d_6$ )  $\delta$  (ppm): 168.06, 164.02, 159.48, 156.33, 156.10, 152.74, 138.82, 137.40, 135.59, 135.10, 130.69, 130.08, 129.69, 129.58, 128.76, 128.75, 128.40, 128.22, 128.21, 126.44, 121.29, 120.88, 119.62, 104.91, 56.03, 32.93, 17.67; Anal. Calcd. For  $C_{34}H_{27}ClN_6O_3S$  (635.14): C, 64.30; H, 4.28; N, 13.23; Found: C, 64.56; H, 4.38; N, 13.57.

***N*-(4-(1-(Hydroxyimino)ethyl)phenyl)-2-((5-(6-methoxy-2-(4-methoxy phenyl)quinolin-4-yl)-4-phenyl-4*H*-1,2,4-triazol-3-yl)thio)- acetamide (7h).**

Yellow solid (0.44 g; 71 % yield); m.p. 182-185 °C;  $^1H$  NMR (500 MHz, DMSO- $d_6$ )  $\delta$  (ppm): 11.10 (s, 1H, OH), 10.55 (s, 1H, NH), 7.96-7.93 (m, 4H, Ar-H), 7.65-7.61 (m, 4H, Ar-H), 7.51 (d,  $J = 6.4$  Hz, 2H, Ar-H), 7.45-7.38 (m, 5H, Ar-H), 7.04 (d,  $J = 8.7$  Hz, 2H, Ar-H), 4.33 (s, 2H, S- $\underline{CH_2}$ ), 3.84 (s, 3H, - $\underline{OCH_3}$ ), 3.82 (s, 3H, - $\underline{OCH_3}$ ), 2.44, 127.70, 126.58, 125.73, 123.16, 120.77, 119.30, 114.74, 103.95, 56.11, 55.77, 37.50, 11.84; Anal. Calcd. For  $C_{35}H_{30}N_6O_4S$  (630.72): C, 66.65; H, 4.79; N, 13.32; Found: C, 66.91; H, 4.86; N, 13.60.

**2-((5-(2-(3,4-Dimethoxyphenyl)-6-methoxyquinolin-4-yl)-4-phenyl-4*H*-1,2,4-triazol-3-yl)thio)-*N*-(4-(1-(hydroxyimino)ethyl)- phenyl)acetamide (7i).**

Yellowish orange solid (0.38 g; 59 % yield); m.p. 177-178 °C; <sup>1</sup>H NMR (500 MHz, DMSO-d<sub>6</sub>) δ (ppm): 11.09 (s, 1H, OH), 10.57 (s, 1H, NH), 7.99 (s, 1H, Ar-H), 7.97 (s, 1H, Ar-H), 7.69-7.63 (m, 5H, Ar-H), 7.56-7.51 (m, 3H, Ar-H), 7.45-7.40 (m, 5H, Ar-H), 7.06 (d, *J* = 8.5 Hz, 1H, Ar-H), 4.34 (s, 2H, S-CH<sub>2</sub>), 3.85 (s, 6H, OCH<sub>3</sub>), 3.82 (s, 3H, OCH<sub>3</sub>), 2.13 (s, 3H, -CH<sub>3</sub>); <sup>13</sup>C NMR (125 MHz, DMSO-d<sub>6</sub>) δ (ppm): 166.09, 158.21, 152.94, 152.85, 152.67, 152.48, 150.78, 149.46, 144.23, 139.62, 133.76, 132.59, 132.14, 131.33, 130.86, 130.48, 130.26, 127.71, 126.58, 125.79, 123.19, 120.96, 120.06, 119.30, 112.23, 110.22, 104.02, 56.12, 56.10, 56.06, 37.46, 11.84; Anal. Calcd. For C<sub>36</sub>H<sub>32</sub>N<sub>6</sub>O<sub>5</sub>S (660.74): C, 65.44; H, 4.88; N, 12.72; Found: C, 65.70; H, 4.79; N, 12.96.

## 4.2. Biological evaluation

**Screening of anti-cancer activity**-Anti-cancer activity of some synthesized compounds was evaluated at the National Institute of Cancer (NCI) against 60 cell lines of different nine cancer cell types. NCI selected 21 Compounds titled **6a**, **6e**, **6g**, **7b-i**, **8a**, **8d-f**, **9a**, **9c** and **9e-h** for *in vitro* anti-cancer screening. The procedures of the assay are described at (<http://www.dtp.nci.nih.gov>). The human cancer cell lines are grown in Roswell Park Memorial Institute medium (RPMI) that contains 5% fetal bovine serum and 2% μM L-glutamine. Cancer cells are inoculated into 96 well microtiter plates in 100 μL at plating densities ranging from 5,000 to 40,000 cells/well depending on the doubling time of individual cell lines. Then microtiter plates are incubated at 37 °C, 5% CO<sub>2</sub>, 95% air and 100% relative humidity for 24 h prior to the addition of the tested compounds. After 24 h, two plates of each cell line are fixed *in situ* with trichloroacetic acid (TCA). The tested compounds were dissolved in dimethyl sulfoxide (DMSO) and stored in the freezer before use. An aliquot of frozen drug concentrate is diluted to the desired concentration with complete medium containing 50μg/mL gentamicin. The compounds were added to the microtiter plates followed by incubation for further 48 h at 37 °C,

5 % CO<sub>2</sub>, 95 % air and 100% relative humidity. Fixation of cancer cell lines is carried out through gentle addition of 50 µL of cold 50 % w/v TCA (final concentration, 10% TCA) then incubated for 60 min. at 4 °C. The plates are washed five times with tap water after getting rid of the supernatant and allowed to dry in air. Sulforhodamine B (SRB) solution (100 µL) at 0.4 % w/v in 1% acetic acid is added to each well, and the plates are incubated for 10 min. at room temperature. The unbound dye is discarded by washing five times with 1% acetic acid, and the plates are air-dried. While the bound stain is subsequently solubilized in 10µM trizma base, and the absorbance is recorded on an automated plate reader at  $\lambda_{\max}$  of 515 nm. The growth percentage is calculated for each of the drug concentrations. Results are expressed as a mean graph of the percent growth of treated cells relative to untreated control as well as to the time zero number of cells.

**STAT3 Displacement Assay** - Following our previously published protocol,<sup>57</sup> 18 mL of 2 µM GST tagged STAT3 were mixed with 2 mL GST-beads (Amersham) and agitated for 1 hour at 4 °C in PBS buffer containing 0.1% β-mercaptoethanol. Then the beads were washed 3 times with 20 mL PBS by spinning down at 2500 rpm for 5 minutes to remove any non-bound STAT3 and re-suspended in 10 ml PBS. 100 µL homogeneous solution of STAT3 bound GST-beads were distributed in each well of Millipore MultiScreen<sub>HTS</sub>, 96-Well Filter Plates (Cat number: MSHVN4B10). 8 wells contained only 100 µL of the buffer were used as a control. Different concentrations of each compound were added to the beads with DMSO concentration adjusted to 2.25% in duplicate. The plates were shaken on an orbital shaker (60 rpm/min) for 30 minutes at room temperature after sealing both the upper surface and the base with aluminum seal (AlumaSeal<sup>TM</sup> CS Films, sigma). 12.5 µM FAM-labeled 5-GpYLPQTV-NH<sub>2</sub> peptide was added to every well, and the shaking continues for another 30 minutes at room temperature. The fluorescence background was adjusted using the wells that contain buffer and peptide. The plates have been transferred to MultiScreen<sub>HTS</sub> Vacuum Manifold, and the resins were washed two times with PBS buffer to remove any unbound labeled peptide and/or compound. Avoid drying the resin during the

washing step. The resins were re-suspended in 100  $\mu$ L PBS buffer, and the plates have been sealed very tightly with aluminum seal. The plates have been inverted upside-down, spinet down at 5000 rpm for 10 minutes until all the resins were settled on the aluminum foil side. The filters were removed then the fluorescence has been measured by a Perkin-Elmer (Waltham, MA) VICTOR3V 1420 multilabel counter plate reader (Excitation filter F485 and emission filter F535). The measured fluorescence ( $\lambda_{535}$ ) is directly proportional to the bound labeled peptide to STAT3. If the compound displaces the peptide, the fluorescence should decrease. The % displacement has been calculated considering the measured fluorescence in the absence of any compound as 0% displacement.

**Cell culture** – A375, 451 Lu-S, and MEL 1617-S melanoma cell lines were cultured in RPMI-1640 medium (Invitrogen) supplemented with 1X Glutamax (Invitrogen). The resistant form of these cell lines (451 Lu-R and MEL 1617-R) were maintained in the same media containing 1  $\mu$ M of PLX4720. Cells were cultured in a humidified 5% CO<sub>2</sub> incubator at 37 °C. For Western blotting, cells were seeded at 800,000-1000,000 cells per well in a 6-well plate and incubated for 24 hours before incubation with or without compounds for 12 hours. Human non-small cell lung cancer cell line (NCI-H157-ATCC CRL-5802) was provided as a gift from Prof. Jonathan M. Kurie lab, The University of Texas MD Anderson Cancer Center, Houston, TX, USA. (A549-ATCC CCL-185) was purchased from the American type culture collection (ATCC; Manassas, VA) and both were maintained in RPMI-1640 medium. The human pancreas ductal adenocarcinoma cell line (MIA PaCa-2 – ATCC CRL-1420) was purchased from ATCC. Human Glioma cell line (U87-MG-ATCC HTB-14) was obtained from the Neurosurgery Tissue Bank, University of California, San Francisco, USA, and both were maintained DMEM medium. The human breast adenocarcinoma cell line (MCF7-ATCC HTB-22) was purchased from ATCC and (MDA-MB-468 – ATCC HTB-132) was provided as a gift from Prof. Chandra Bartholomeusz lab, The University of Texas MD Anderson Cancer Center, Houston, TX, USA. and both were cultured in DMEM/F12 medium. All media were supplemented with FBS (FBS; 10%; US-

Origin, heat-inactivated, Life Technologies), 100 U ml<sup>-1</sup> penicillin, and 100 µg ml<sup>-1</sup> streptomycin (Life Technologies) and maintained in a 37 °C incubator with 5% CO<sub>2</sub>.

**Western Blotting** - After 12 hours of drug incubation, cell lysates were prepared in M-PER™ Mammalian Protein Extraction Reagent (Thermo-Fisher) after washing in PBS (Invitrogen). The lysates were cleared by centrifugation, and Bradford analysis (Bio-Rad) was used to measure the protein concentration. Lysates containing 60 µg of total protein were fractionated on a 10% SDS polyacrylamide gel (Bio-Rad) and transferred to Hybond-P PVDF Membrane (GE Healthcare). Primary antibodies were incubated overnight at 4 °C using 1: 1,000 antiphospho-Stat3 (Tyr-705), rabbit mAb (Cell Signaling Technology); 1:1000 anti-phospho-Stat3 (Ser727) rabbit polyclonal Ab (Cell Signaling Technology); 1:1000 anti-Stat3 (124H6) mouse mAb (Cell Signaling Technology); 1:1000 anti-PARP (46D11) rabbit mAb (Cell Signaling Technology); 1:1000 anti-cleaved-PARP (D214) rabbit polyclonal Abs (Cell Signaling Technology); 1:1000 anti-Caspase-7 rabbit polyclonal Abs (Cell Signaling Technology); 1:10000 anti-PAX3 (16H22L10) ABfinity rabbit mAb (Invitrogen); 1:1000 anti-Cyclin D1 (DCS6) mouse mAb (Cell Signaling Technology); 1:1000 anti p27 Kip1 (D69C12) XP rabbit mAb (Cell Signaling Technology); 1:1000 anti-phospho-Jak2 (Tyr1007/1008) rabbit antibody (Cell Signaling Technology); 1:1000 anti-Jak2 (D2E12) XP® rabbit mAb (Cell Signaling Technology); 1:1000 anti-Src (L4A1) mouse mAb (Cell Signaling Technology), 1:1000 anti-Phospho-Src Family (Tyr416) rabbit antibody (Cell Signaling Technology); 1:1000 anti-Phospho-Stat1 (Tyr701) (D4A7) rabbit mAb (Cell Signaling Technology); 1:1000 anti-Stat1 (D1K9Y) rabbit mAb (Cell Signaling Technology), 1:1000 anti-Phospho-Stat5 (Tyr694) (D47E7) XP® rabbit mAb (Cell Signaling Technology), 1:1000 anti-Stat5 (D2O6Y) rabbit mAb (Cell Signaling Technology); 1:1000 anti-Phospho-Stat6 (Tyr641) antibody (Cell Signaling Technology); 1:1000 anti-Stat6 (D3H4) rabbit mAb (Cell Signaling Technology); 1/2000 anti-Vinculin (E1E9V) XP rabbit mAb (Cell

Signaling Technology) and 1:5000 anti-actin, clone 4 mouse mAb (Millipore). Either anti-rabbit (Bio-Rad) or anti-mouse (Cell Signaling Technology) horseradish peroxidase-conjugated secondary antibodies and Western Bright ECL Western Blotting Reagents (Advansta) were used to develop the blots. All experiments were reproduced in independent experiments. All experiments were performed two times.

**STAT3 Reporter Assay** - Cignal STAT3 Reporter (luc) Kit: CCS-9028L was used in this assay according to the reported protocol ([www.sabiosciences.com](http://www.sabiosciences.com)). The Cignal Reporter Assays (luc) include pre-formulated, transfection-ready reporter, negative control, and positive control. Cells were seeded in white (clear bottom) 96-well plate and transfected with a mixture of inducible STAT3-responsive firefly luciferase construct and constitutively expressing Renilla luciferase construct (40:1) using Lipofectamine 3000 reagent (following manufacturer protocol-Invitrogen), after 48 hours of transfection, cells were treated with different doses of each inhibitor with vehicle (DMSO) for 12 hours. Dual-luciferase assay was performed using Promega dual luciferase assay reagent. The change in the activity of each signaling pathway is determined by comparing the normalized luciferase activities of the reporter in treated versus untreated cells. The identically treated negative control transfectants serve as a specificity control. The positive control serves as a control for transfection efficiency by monitoring GFP expression, as well as a positive control for both the firefly and Renilla luciferase assays.

**Cell growth and proliferation assays** - The MTS assay (CellTiter 96® Aqueous One Solution Cell Proliferation Assay from Promega) was used to detect the viability and/or proliferation of cells following the manufacturer protocol. All experiments were performed in triplicate.

**ROS production assessment by flow cytometry** - 1X106 A375 cells were seeded in 60 mm plate and incubated overnight to settle. Next day cells were treated with either DMSO, 10, or 25

$\mu\text{M}$  7b in full RPMI medium for 18 hours. Cells were digested with trypsin, and washed three times with PBS and incubated with a final concentration of  $10\ \mu\text{M}$  DCFH-DA (2', 7'-dichlorofluorescein diacetate, ROS-sensitive dye) for 30 min at  $37\ ^\circ\text{C}$  in the dark with a density of  $1 \times 10^6$  cells/mL. Cells were washed two times in pre-warmed DPBS before resuspension in DPBS. The fluorescence was detected by flow cytometry (488 nm laser for excitation and detected by 535 nm filter) using BD LSR Fortessa SORP Flow Cytometer. Data were processed using FlowJo v10 (Tree Star, Inc., Ashland, OR, USA) software.

**Colony formation assay** - A375 cells were plated (2500 cells per well) in 6-well plate containing RPMI media with 5% FBS. Cells were allowed to settle overnight then treated with different doses of 7b or 7c. Cells were allowed to grow for 14 days, then fixed for 15 min in 4% paraformaldehyde and stained with 0.2% crystal violet (in 20% methanol) for 10 min. Cells were washed several times with PBS before imaging.

**Immunofluorescence study** – 2000 MEF (Mouse Embryonic Fibroblast) cells were seeded in each well of a 96-well black plate with clear bottom. Cells were incubated to adhere for 24 hours and then incubated with different doses of each inhibitor in serum-free media for another night before induction by full RPMI media containing 100 nM EGF for 30 minutes. Cells were washed by PBS, fixed by 4% paraformaldehyde in PBS for 10 min at room temperature. The cells were permeabilized with 0.2% Triton X-100 for 5 min and blocked with 10% Goat serum (Cell Signaling Technology). Immunostaining was performed by incubating cells with monoclonal anti-STAT3 antibody produced in mouse (124H6) (Cell signaling Tech), followed by anti-mouse IgG (H+L), F(ab')<sub>2</sub> Fragment (Alexa Fluor<sup>®</sup>488 Conjugate) (Cell signaling Tech). DAPI (4',6'-diamidino-2-phenylindole) was included in the mounting medium as a counterstain for nuclei. Cells were visualized and quantified using the Cytation 5 cell imaging system.

**IncuCyte single-cell apoptosis analysis** - 2000 451 Lu-R cells were seeded in each well of 96 well plates, cells were left for 24 hours to adhere then treated with different doses of **7b** in full media with a constant concentration of the IncuCyte Caspase-3/7 reagent. Cells were incubated and imaged in the IncuCyte® ZOOM equipment with a  $\times 10$  objective at different time points. The number of apoptotic cells was normalized to the percentage confluency at the final time point to account for cell proliferation.

**Cell Cycle Analysis** - A375 cells were treated with DMSO, 10, or 25  $\mu\text{M}$  of **7b** or **7c** for 24 hrs. in full media. Cells were harvested and washed twice with phosphate-buffered saline (PBS) and fixed in ice-cold 70% ethanol overnight at  $-20^{\circ}\text{C}$  as previously described. The next day, cells were washed two times with PBS and re-suspended in Propidium Iodide (PI)/RNase Staining Solution (cell signaling Cat # 4087) for 30 minutes at room temperature, light-protected. Cell-cycle analysis was performed using BD LSRFortessa SORP Flow Cytometer. Data obtained from the cell cycle distributions were analyzed using both FlowJo v10 (Tree Star, Inc., Ashland, OR, USA) software FlowJo v10 was employed to estimate the percentage of cells in G1, S, and G2.

**Measurement of NO release** - The amount of nitric oxide released was determined using Griess Reagent Kit for Nitrite Determination (Molecular Probes, Eugene, Oregon. kit no. G-7921).<sup>58</sup> 280  $\mu\text{L}$  of the nitrite-containing sample (100  $\mu\text{M}$  of each compound in a solution of either phosphate buffer (pH 7.4) or 0.1 N HCl (pH 1), 5 mM DTT and 2% DMSO) were added in each well of a microplate. The mixture was incubated for different time points at room temperature, then 20  $\mu\text{L}$  of Griess Reagent (equal volumes of N-(1-naphthyl)ethylenediamine and sulfanilic acid) was added. After 30 minutes, the absorbance of the nitrite-containing samples was measured at 548 nm relative to the reference sample that contains 20  $\mu\text{L}$  of Griess Reagent and

280  $\mu$ L of phosphate buffer (pH 7.4), 2 mM DTT and 1% DMSO. Sodium nitrite solutions were prepared at different concentrations to construct the calibration curve. The amount of NO released (mol/mol) was measured relative to the amount of NO released from standard sodium nitrite solutions.

**Nuclear extract preparation and gel shift assays** - A375 cells were seeded in 60 mm plate then treated overnight with different concentrations of 7b, 7c, or DMSO in full RPMI media. The cells were harvested, and the nuclear extract was prepared as previously described.<sup>59</sup> After washing the cells with PBS, cells were suspended in 250  $\mu$ L low salt lysis buffer containing 10 mM Hepes (pH 8), 10 mM NaCl, 5 mM MgCl<sub>2</sub>, and 0.5 mM DTT. Cells were incubated in ice for 30 minutes, nuclei were pelleted by centrifugation at 1200g for 4 minutes, supernatant was discarded and 25  $\mu$ L of high salt lysis buffer (10 mM Hepes pH 8, 300 mM KCl, 5 mM MgCl<sub>2</sub>, 0.5 mM DTT, 20% glycerol) was added to the pellets to extract the nucleus. The tubes were incubated in a rotating wheel for 30 minutes at 4°C before centrifugation for 20 minutes at 11000 g. The protein content of the supernatant was quantified using Bradford reagent, and 5  $\mu$ g were used for each EMSA reaction. All buffers were supplemented with 1X Complete EDTA-free Protease Inhibitors Cocktail and PhosSTOP Phosphatase Inhibitors Cocktail (Roche Diagnostics). EMSA analysis was carried out using IRDye® 700 STAT3 Consensus Oligonucleotide following the manufacture protocol (Cat. Number 829-07922, LI-COR Biosciences). Stat3 Consensus and Mutant Oligonucleotides were purchased from Santa Cruze Biotechnologies (Cat. numbers # sc-2571 and sc-2572).

**Docking Studies** - Docking was carried out with AutoDock 4.2<sup>60</sup>. The atomic coordinate of the STAT3-SH2 domain (res586-688) (PDB ID: 1BG1)<sup>28</sup> was used as the receptor model for docking. Docking was carried out centered at Gln635 with a grid box of 100  $\times$  100  $\times$  100 points

in three dimensions with a spacing of 0.375 Å. The charges of proteins were assigned using the PDB2PQR<sup>61</sup> server, and electrostatic potential was calculated using APBS<sup>62</sup>. The electrostatic potential varied from  $-5K_B T/e$  to  $+5K_B T/e$  and was depicted using Chimera<sup>63</sup> in panels A and B from red to blue, respectively.

## 5. Acknowledgment.

This research has been supported by the Faculty of Pharmacy, Minia University, Minia, Egypt, the Welch Foundation F-1390 (to K.N.D.) and Cancer Prevention and Research Institute of Texas, USA grant RP140649 (to K.N.D.). The authors would like to thank Prof. Kenneth Tsai, H. Lee Moffitt Cancer Center & Research Institute, Florida, USA, for providing the four tested melanoma cell lines.

## 6. Supplementary Data.

Supplementary data to this article include the spectral analysis data for all the synthesized compounds.

## 7. References

1. Chabner, B. A., Biological basis for cancer treatment. *Ann Intern Med* **1993**, *118* (8), 633-7.
2. Russo, A. E.; Torrisi, E.; Bevelacqua, Y.; Perrotta, R.; Libra, M.; McCubrey, J. A.; Spandidos, D. A.; Stivala, F.; Malaponte, G., Melanoma: molecular pathogenesis and emerging target therapies (Review). *Int J Oncol* **2009**, *34* (6), 1481-9.
3. Liu, F.; Cao, J.; Wu, J.; Sullivan, K.; Shen, J.; Ryu, B.; Xu, Z.; Wei, W.; Cui, R., Stat3-targeted therapies overcome the acquired resistance to vemurafenib in melanomas. *J Invest Dermatol* **2013**, *133* (8), 2041-9.
4. Furtek, S. L.; Backos, D. S.; Matheson, C. J.; Reigan, P., Strategies and Approaches of Targeting STAT3 for Cancer Treatment. *ACS Chem Biol* **2016**, *11* (2), 308-18.
5. Xiong, A.; Yang, Z.; Shen, Y.; Zhou, J.; Shen, Q., Transcription Factor STAT3 as a Novel Molecular Target for Cancer Prevention. *Cancers (Basel)* **2014**, *6* (2), 926-57.
6. Wen, Z.; Zhong, Z.; Darnell, J. E., Jr., Maximal activation of transcription by Stat1 and Stat3 requires both tyrosine and serine phosphorylation. *Cell* **1995**, *82* (2), 241-50.

7. Niu, G.; Heller, R.; Catlett-Falcone, R.; Coppola, D.; Jaroszeski, M.; Dalton, W.; Jove, R.; Yu, H., Gene therapy with dominant-negative Stat3 suppresses growth of the murine melanoma B16 tumor in vivo. *Cancer Res* **1999**, *59* (20), 5059-63.
8. Kortylewski, M.; Jove, R.; Yu, H., Targeting STAT3 affects melanoma on multiple fronts. *Cancer Metastasis Rev* **2005**, *24* (2), 315-27.
9. Xie, T. X.; Wei, D.; Liu, M.; Gao, A. C.; Ali-Osman, F.; Sawaya, R.; Huang, S., Stat3 activation regulates the expression of matrix metalloproteinase-2 and tumor invasion and metastasis. *Oncogene* **2004**, *23* (20), 3550-60.
10. Becker, T. M.; Boyd, S. C.; Mijatov, B.; Gowrishankar, K.; Snoyman, S.; Pupo, G. M.; Scolyer, R. A.; Mann, G. J.; Kefford, R. F.; Zhang, X. D.; Rizos, H., Mutant B-RAF-Mcl-1 survival signaling depends on the STAT3 transcription factor. *Oncogene* **2014**, *33* (9), 1158-66.
11. Chapman, P. B.; Hauschild, A.; Robert, C.; Haanen, J. B.; Ascierto, P.; Larkin, J.; Dummer, R.; Garbe, C.; Testori, A.; Maio, M.; Hogg, D.; Lorigan, P.; Lebbe, C.; Jouary, T.; Schadendorf, D.; Ribas, A.; O'Day, S. J.; Sosman, J. A.; Kirkwood, J. M.; Eggermont, A. M.; Dreno, B.; Nolop, K.; Li, J.; Nelson, B.; Hou, J.; Lee, R. J.; Flaherty, K. T.; McArthur, G. A., Improved survival with vemurafenib in melanoma with BRAF V600E mutation. *N Engl J Med* **2011**, *364* (26), 2507-16.
12. Flaherty, K. T.; Infante, J. R.; Daud, A.; Gonzalez, R.; Kefford, R. F.; Sosman, J.; Hamid, O.; Schuchter, L.; Cebon, J.; Ibrahim, N.; Kudchadkar, R.; Burris, H. A., 3rd; Falchook, G.; Algazi, A.; Lewis, K.; Long, G. V.; Puzanov, I.; Lebowitz, P.; Singh, A.; Little, S.; Sun, P.; Allred, A.; Ouellet, D.; Kim, K. B.; Patel, K.; Weber, J., Combined BRAF and MEK Inhibition in Melanoma with BRAF V600 Mutations. *N Engl J Med* **2012**.
13. Flaherty, K. T.; Puzanov, I.; Kim, K. B.; Ribas, A.; McArthur, G. A.; Sosman, J. A.; O'Dwyer, P. J.; Lee, R. J.; Grippo, J. F.; Nolop, K.; Chapman, P. B., Inhibition of mutated, activated BRAF in metastatic melanoma. *N Engl J Med* **2010**, *363* (9), 809-19.
14. Long, G. V.; Trefzer, U.; Davies, M. A.; Kefford, R. F.; Ascierto, P. A.; Chapman, P. B.; Puzanov, I.; Hauschild, A.; Robert, C.; Algazi, A.; Mortier, L.; Tawbi, H.; Wilhelm, T.; Zimmer, L.; Switzky, J.; Swann, S.; Martin, A.-M.; Guckert, M.; Goodman, V.; Streit, M.; Kirkwood, J. M.; Schadendorf, D., Dabrafenib in patients with Val600Glu or Val600Lys BRAF-mutant melanoma metastatic to the brain (BREAK-MB): a multicentre, open-label, phase 2 trial. *The Lancet Oncology* **2012**, *13* (11), 1087-1095.
15. Notarangelo, T.; Sisinni, L.; Trino, S.; Calice, G.; Simeon, V.; Landriscina, M., IL6/STAT3 axis mediates resistance to BRAF inhibitors in thyroid carcinoma cells. *Cancer Lett* **2018**, *433*, 147-155.
16. Chen, J.; Bai, L.; Bernard, D.; Nikolovska-Coleska, Z.; Gomez, C.; Zhang, J.; Yi, H.; Wang, S., Structure-Based Design of Conformationally Constrained, Cell-Permeable STAT3 Inhibitors. *ACS Med Chem Lett* **2010**, *1* (2), 85-89.
17. Mandal, P. K.; Gao, F.; Lu, Z.; Ren, Z.; Ramesh, R.; Birtwistle, J. S.; Kaluarachchi, K. K.; Chen, X.; Bast, R. C., Jr.; Liao, W. S.; McMurray, J. S., Potent and selective phosphopeptide mimetic prodrugs targeted to the Src homology 2 (SH2) domain of signal transducer and activator of transcription 3. *J Med Chem* **2011**, *54* (10), 3549-63.
18. Miyoshi, K.; Takaishi, M.; Nakajima, K.; Ikeda, M.; Kanda, T.; Tarutani, M.; Iiyama, T.; Asao, N.; DiGiovanni, J.; Sano, S., Stat3 as a therapeutic target for the treatment of psoriasis: a clinical feasibility study with STA-21, a Stat3 inhibitor. *J Invest Dermatol* **2011**, *131* (1), 108-17.
19. Wong, A. L. A.; Hirpara, J. L.; Pervaiz, S.; Eu, J. Q.; Sethi, G.; Goh, B. C., Do STAT3 inhibitors have potential in the future for cancer therapy? *Expert Opin Investig Drugs* **2017**, *26* (8), 883-887.

20. Song, H.; Wang, R.; Wang, S.; Lin, J., A low-molecular-weight compound discovered through virtual database screening inhibits Stat3 function in breast cancer cells. *Proc Natl Acad Sci U S A* **2005**, *102* (13), 4700-5.
21. Duan, Y. C.; Ma, Y. C.; Zhang, E.; Shi, X. J.; Wang, M. M.; Ye, X. W.; Liu, H. M., Design and synthesis of novel 1,2,3-triazole-dithiocarbamate hybrids as potential anticancer agents. *Eur J Med Chem* **2013**, *62*, 11-9.
22. Becerril, J. L.; Benitez, J. G.; Juarez, J. J.; Banales, J. M.; Zeron, H. M.; Navarro, M. D., Evaluation of the Effect of 1,3-Bis(4-Phenyl)-1H-1,2,3-Triazolyl-2-Propanolol on Gene Expression Levels of JAK2-STAT3, NF-kappaB, and SOCS3 in Cells Cultured from Biopsies of Mammary Lesions. *Biochem Genet* **2015**, *53* (11-12), 291-300.
23. Hou, Y. P.; Sun, J.; Pang, Z. H.; Lv, P. C.; Li, D. D.; Yan, L.; Zhang, H. J.; Zheng, E. X.; Zhao, J.; Zhu, H. L., Synthesis and antitumor activity of 1,2,4-triazoles having 1,4-benzodioxan fragment as a novel class of potent methionine aminopeptidase type II inhibitors. *Bioorg Med Chem* **2011**, *19* (20), 5948-54.
24. Lee, S. M.; Yoon, K. B.; Lee, H. J.; Kim, J.; Chung, Y. K.; Cho, W. J.; Mukai, C.; Choi, S.; Kang, K. W.; Han, S. Y.; Ko, H.; Kim, Y. C., The discovery of 2,5-isomers of triazole-pyrrolopyrimidine as selective Janus kinase 2 (JAK2) inhibitors versus JAK1 and JAK3. *Bioorg Med Chem* **2016**, *24* (21), 5036-5046.
25. Huang, Z.; Fu, J.; Zhang, Y., Nitric Oxide Donor-Based Cancer Therapy: Advances and Prospects. *J Med Chem* **2017**, *60* (18), 7617-7635.
26. Chen, H.; Yang, Z.; Ding, C.; Chu, L.; Zhang, Y.; Terry, K.; Liu, H.; Shen, Q.; Zhou, J., Fragment-based drug design and identification of HJC0123, a novel orally bioavailable STAT3 inhibitor for cancer therapy. *Eur J Med Chem* **2013**, *62*, 498-507.
27. Matsuno, K.; Masuda, Y.; Uehara, Y.; Sato, H.; Muroya, A.; Takahashi, O.; Yokotagawa, T.; Furuya, T.; Okawara, T.; Otsuka, M.; Ogo, N.; Ashizawa, T.; Oshita, C.; Tai, S.; Ishii, H.; Akiyama, Y.; Asai, A., Identification of a New Series of STAT3 Inhibitors by Virtual Screening. *ACS Med Chem Lett* **2010**, *1* (8), 371-5.
28. Becker, S.; Groner, B.; Muller, C. W., Three-dimensional structure of the Stat3beta homodimer bound to DNA. *Nature* **1998**, *394* (6689), 145-51.
29. Trott, O.; Olson, A. J., AutoDock Vina: improving the speed and accuracy of docking with a new scoring function, efficient optimization, and multithreading. *J Comput Chem* **2010**, *31* (2), 455-61.
30. Thomas, D. D.; Ridnour, L. A.; Isenberg, J. S.; Flores-Santana, W.; Switzer, C. H.; Donzelli, S.; Hussain, P.; Vecoli, C.; Paolocci, N.; Ambs, S.; Colton, C. A.; Harris, C. C.; Roberts, D. D.; Wink, D. A., The chemical biology of nitric oxide: implications in cellular signaling. *Free Radic Biol Med* **2008**, *45* (1), 18-31.
31. Zhang, X.; Sun, Y.; Pireddu, R.; Yang, H.; Urlam, M. K.; Lawrence, H. R.; Guida, W. C.; Lawrence, N. J.; Sebt, S. M., A novel inhibitor of STAT3 homodimerization selectively suppresses STAT3 activity and malignant transformation. *Cancer Res* **2013**, *73* (6), 1922-33.
32. Liu, L.; Nam, S.; Tian, Y.; Yang, F.; Wu, J.; Wang, Y.; Scuto, A.; Polychronopoulos, P.; Magiatis, P.; Skaltsounis, L.; Jove, R., 6-Bromindirubin-3'-oxime inhibits JAK/STAT3 signaling and induces apoptosis of human melanoma cells. *Cancer Res* **2011**, *71* (11), 3972-9.
33. Yu, W.; Li, C.; Zhang, W.; Xia, Y.; Li, S.; Lin, J. Y.; Yu, K.; Liu, M.; Yang, L.; Luo, J.; Chen, Y.; Sun, H.; Kong, L., Discovery of an Orally Selective Inhibitor of Signal Transducer and Activator of

- Transcription 3 Using Advanced Multiple Ligand Simultaneous Docking. *J Med Chem* **2017**, *60* (7), 2718-2731.
34. Bartolowits, M. D.; Brown, W.; Ali, R.; Pedley, A. M.; Chen, Q.; Harvey, K. E.; Wendt, M. K.; Davisson, V. J., Selective Inhibition of STAT3 Phosphorylation Using a Nuclear-Targeted Kinase Inhibitor. *ACS Chem Biol* **2017**, *12* (9), 2371-2378.
  35. Guo, J.; Yu, W.; Cai, G.; Zhang, W.; Li, S.; Zhu, J.; Song, D.; Kong, L., Discovery of new benzensulfonamide derivatives as tripedal STAT3 inhibitors. *Eur J Med Chem* **2018**, *151*, 752-764.
  36. Li, C.; Chen, C.; An, Q.; Yang, T.; Sang, Z.; Yang, Y.; Ju, Y.; Tong, A.; Luo, Y., A novel series of napabucasin derivatives as orally active inhibitors of signal transducer and activator of transcription 3 (STAT3). *Eur J Med Chem* **2019**, *162*, 543-554.
  37. Huang, W.; Liu, Y.; Wang, J.; Yuan, X.; Jin, H. W.; Zhang, L. R.; Zhang, J. T.; Liu, Z. M.; Cui, J. R., Small-molecule compounds targeting the STAT3 DNA-binding domain suppress survival of cisplatin-resistant human ovarian cancer cells by inducing apoptosis. *Eur J Med Chem* **2018**, *157*, 887-897.
  38. Gough, D. J.; Marie, I. J.; Lobry, C.; Aifantis, I.; Levy, D. E., STAT3 supports experimental K-RasG12D-induced murine myeloproliferative neoplasms dependent on serine phosphorylation. *Blood* **2014**, *124* (14), 2252-61.
  39. Timofeeva, O. A.; Gaponenko, V.; Lockett, S. J.; Tarasov, S. G.; Jiang, S.; Michejda, C. J.; Perantoni, A. O.; Tarasova, N. I., Rationally designed inhibitors identify STAT3 N-domain as a promising anticancer drug target. *ACS Chem Biol* **2007**, *2* (12), 799-809.
  40. Watson, J. V.; Chambers, S. H.; Smith, P. J., A pragmatic approach to the analysis of DNA histograms with a definable G1 peak. *Cytometry* **1987**, *8* (1), 1-8.
  41. Xiong, H.; Zhang, Z. G.; Tian, X. Q.; Sun, D. F.; Liang, Q. C.; Zhang, Y. J.; Lu, R.; Chen, Y. X.; Fang, J. Y., Inhibition of JAK1, 2/STAT3 signaling induces apoptosis, cell cycle arrest, and reduces tumor cell invasion in colorectal cancer cells. *Neoplasia* **2008**, *10* (3), 287-97.
  42. Lee, H. J.; Zhuang, G.; Cao, Y.; Du, P.; Kim, H. J.; Settleman, J., Drug resistance via feedback activation of Stat3 in oncogene-addicted cancer cells. *Cancer Cell* **2014**, *26* (2), 207-21.
  43. Villanueva, J.; Vultur, A.; Lee, J. T.; Somasundaram, R.; Fukunaga-Kalabis, M.; Cipolla, A. K.; Wubbenhorst, B.; Xu, X.; Gimotty, P. A.; Kee, D.; Santiago-Walker, A. E.; Letrero, R.; D'Andrea, K.; Pushparajan, A.; Hayden, J. E.; Brown, K. D.; Laquerre, S.; McArthur, G. A.; Sosman, J. A.; Nathanson, K. L.; Herlyn, M., Acquired resistance to BRAF inhibitors mediated by a RAF kinase switch in melanoma can be overcome by cotargeting MEK and IGF-1R/PI3K. *Cancer Cell* **2010**, *18* (6), 683-95.
  44. Muscia, G. C.; Carnevale, J. P.; Bollini, M.; Asís, S. E., Microwave-assisted döbner synthesis of 2-phenylquinoline-4-carboxylic acids and their antiparasitic activities. *Journal of Heterocyclic Chemistry* **2008**, *45* (2), 611-614.
  45. El-Feky, S. A.; Abd El-Samii, Z. K.; Osman, N. A.; Lashine, J.; Kamel, M. A.; Thabet, H., Synthesis, molecular docking and anti-inflammatory screening of novel quinoline incorporated pyrazole derivatives using the Pfitzinger reaction II. *Bioorg Chem* **2015**, *58*, 104-16.
  46. Trikojus, V. M.; White, D. E., Derivatives of 2-phenyl quinoline, Part I. Preparation of some "atophans" from ventric aldehyde. . *Journal and Proceedings of the Royal Society of New South Wales* **1932**, *66*, 273-278.

47. Xu, Z.-h.; Xi, P.-x.; Chen, F.-j.; Liu, X.-h.; Zeng, Z.-z., Synthesis, characterization, and DNA-binding properties of copper(II), cobalt(II), and nickel(II) complexes with salicylaldehyde 2-phenylquinoline-4-carboylhydrazone. *Transition Metal Chemistry* **2008**, *33* (2), 267-273.
48. Leardini, R.; Pedulli, G. F.; Tundo, A.; Zanardi, G., Aromatic annelation by reaction of arylimidoyl radicals with alkynes: a new synthesis of quinolines. *Journal of the Chemical Society, Chemical Communications* **1984**, (20), 1320-1321.
49. Zemtsova, M. N.; Zimichev, A. V.; Trakhtenberg, P. L.; Klimochkin, Y. N.; Leonova, M. V.; Balakhnin, S. M.; Bormotov, N. I.; Serova, O. A.; Belanov, E. F., Synthesis and antiviral activity of several quinoline derivatives. *Pharmaceutical Chemistry Journal* **2011**, *45* (5), 267.
50. Raulfs, F. W.; Mayer, U., Quinoline-4-carboxylic acid derivatives and their use as color formers. *Eur. Pat. Appl* **1990**, EP 384313 A1 19900829.
51. Xu, Z. H.; Xi, P. X.; Chen, F. J.; Zeng, Z. Z., Synthesis, characterization, and DNA-binding of Ln(III) complexes with 2-hydroxybenzylidene-2-phenylquinoline-4-carbonylhydrazone. *Journal of Coordination Chemistry* **2009**, *62* (13), 2193-2202.
52. Metwally, K. A.; Abdel-Aziz, L. M.; Lashine el, S. M.; Hussein, M. I.; Badawy, R. H., Hydrazones of 2-aryl-quinoline-4-carboxylic acid hydrazides: synthesis and preliminary evaluation as antimicrobial agents. *Bioorg Med Chem* **2006**, *14* (24), 8675-82.
53. Mohassab, A. M.; Hassan, H. A.; Abdelhamid, D.; Abdel-Aziz, M.; Dalby, K. N.; Kaoud, T. S., Novel quinoline incorporating 1,2,4-triazole/oxime hybrids: Synthesis, molecular docking, anti-inflammatory, COX inhibition, ulcerogenicity and histopathological investigations. *Bioorg Chem* **2017**, *75*, 242-259.
54. El-Aal, H. A. A.; El-Emary, T. I., Efficient synthesis, characterization and biological evaluation of some new atophan carbohydrazone derivatives *Journal of Chemical and Pharmaceutical Research* **2014**, *6* (12), 90-99.
55. Xie, H.; Ng, D.; Savinov, S. N.; Dey, B.; Kwong, P. D.; Wyatt, R.; Smith, A. B., 3rd; Hendrickson, W. A., Structure-activity relationships in the binding of chemically derivatized CD4 to gp120 from human immunodeficiency virus. *J Med Chem* **2007**, *50* (20), 4898-908.
56. Abd-Ellah, H. S.; Abdel-Aziz, M.; Shoman, M. E.; Beshr, E. A.; Kaoud, T. S.; Ahmed, A. F., Novel 1,3,4-oxadiazole/oxime hybrids: Synthesis, docking studies and investigation of anti-inflammatory, ulcerogenic liability and analgesic activities. *Bioorg Chem* **2016**, *69*, 48-63.
57. Kaoud, T. S.; Yan, C.; Mitra, S.; Tseng, C. C.; Jose, J.; Taliaferro, J. M.; Tuohetahuntala, M.; Devkota, A.; Sammons, R.; Park, J.; Park, H.; Shi, Y.; Hong, J.; Ren, P.; Dalby, K. N., From in Silico Discovery to intra-Cellular Activity: Targeting JNK-Protein Interactions with Small Molecules. *ACS Med Chem Lett* **2012**, *3* (9), 721-725.
58. Sun, J.; Zhang, X.; Broderick, M.; Fein, H., Measurement of Nitric Oxide Production in Biological Systems by Using Griess Reaction Assay. *Sensors* **2003**, *3* (8), 276-284.
59. Sancisi, V.; Gandolfi, G.; Ambrosetti, D. C.; Ciarrocchi, A., Histone Deacetylase Inhibitors Repress Tumoral Expression of the Proinvasive Factor RUNX2. *Cancer Research* **2015**, *75* (9), 1868-1882.
60. Morris, G. M.; Huey, R.; Lindstrom, W.; Sanner, M. F.; Belew, R. K.; Goodsell, D. S.; Olson, A. J., AutoDock4 and AutoDockTools4: Automated docking with selective receptor flexibility. *J Comput Chem* **2009**, *30* (16), 2785-91.

61. Dolinsky, T. J.; Nielsen, J. E.; McCammon, J. A.; Baker, N. A., PDB2PQR: an automated pipeline for the setup of Poisson-Boltzmann electrostatics calculations. *Nucleic Acids Res* **2004**, *32* (Web Server issue), W665-7.
62. Baker, N. A.; Sept, D.; Joseph, S.; Holst, M. J.; McCammon, J. A., Electrostatics of nanosystems: application to microtubules and the ribosome. *Proc Natl Acad Sci U S A* **2001**, *98* (18), 10037-41.
63. Pettersen, E. F.; Goddard, T. D.; Huang, C. C.; Couch, G. S.; Greenblatt, D. M.; Meng, E. C.; Ferrin, T. E., UCSF Chimera--a visualization system for exploratory research and analysis. *Journal of computational chemistry* **2004**, *25* (13), 1605-12.

Journal Pre-proof

Highlights:

- Design and synthesis of hybrid compounds containing dual-functional NO-releasing STAT3 inhibitors.
- They inhibited STAT3 phosphorylation in several cancer cell lines without affecting other STAT isoforms.
- They abrogated STAT3 nuclear translocation, DNA binding, and transcriptional activity in cancer cells.
- They exhibited higher sensitivity towards cancer cells carrying a BRAF mutation, induced ROS production, cell cycle arrest, and apoptosis.
- They showed comparable cytotoxicity towards both SB-590885-sensitive and resistant melanoma cell lines.

**Declaration of interests**

The authors declare that they have no known competing financial interests or personal relationships that could have appeared to influence the work reported in this paper.

The authors declare the following financial interests/personal relationships which may be considered as potential competing interests:

Journal Pre-proof